# Integrity of a Wellbore for Methane Gas Production

by

Marilena Papadopoulou (mp627)

Fourth-year undergraduate project in
Group D, 2014/2015

I hereby declare that, except where specifically indicated, the work submitted herein is my own original work.

Signed: ______________________________ Date: _______________

# Contents

# Nomenclature

## Roman Symbols

| | |
|---|---|
| $d$ | Depth into Depressurization Zone |
| $d_{pl}$ | Depth of Plastic Region of the Casing |
| $e$ | Void Ratio |
| $i$ | Trough width |
| $K^{'}$ | Bulk Modulus |
| $M$ | Slope of critical state line |
| $n$ | Porosity |
| $p^{'}$ | Mean Effective Stress |
| $p^{'}_{cc}$ | Hardening parameter of cohesion |
| $p^{'}_{cd}$ | Hardening parameter of dilation |
| $p^{'}_{cs}$ | Volumetric Yield Stress |
| $R$ | Radius From the Centreline of the Wellbore |
| $R_i$ | Distance of Pore Pressure Reduction |
| $S_h$ | Hydrate Saturation |
| $S_{max}$ | Maximum Settlement of the Bottom of the Casing |
| v | Specific Volume |

## Greek Symbols

| | |
|---|---|
| $\epsilon_p$ | Plastic Strain |
| $\kappa$ | Slope of a swelling line |
| $\lambda$ | Slope of a normal compression line |
| $\nu$ | Poisson's Ratio |
| $\rho$ | Density |
| $\sigma$ | Tensile Stress |
| $\Phi$ | Friction Angle |
| $\psi$ | Dilation Angle |

# 1 Introduction

## 1.1 Background

Many studies have shown that the worldwide amount of gas found in gas hydrates is enormous and that there is more energy in gas hydrates than in all the world's oil, coal and gas put together. It is currently estimated that the quantity of hydrocarbons in gas hydrates is of the order of $10^{15}$ to $10^{18}$ cubic meters [1], [2], [3]. Therefore the attractiveness of gas hydrates as a potential energy resource arises from the abundance of their worldwide existence.

Natural gas hydrates also referred to as clathrates (as no hydrogen bonding occurs between gas molecules and water molecules) are crystalline formations of water and gaseous molecules. Gas molecules occupy cages (cavities) within the crystal structure of water [4]. The most common gas in hydrates is methane [5].

Hydrates store large amounts of methane gas in relatively small volume. Typically, one cubic meter of the compound can release about 164 cubic meters of methane and 0.87 cubic meters of water, making it a highly energy intensive fuel [6]. Due to these, together with the abundant reserves, methane has been recognized as a potential energy resource and has attracted interest from many governments and energy companies.

However, (just as with shale gas and conventional hydrocarbons, for that matter), not all of this potential energy resource will prove technically recoverable, but even if only a small portion of it is commercially extracted that would still be a significantly huge amount [7]. Therefore, methane gas can be very promising of a revolution in the energy resource sector in the future, providing that a cost-effective production method can be developed.

The extraction process from methane hydrates though, makes the design of wellbores in such deep offshore fields even more challenging than conventional natural gas. The degradation of the mechanical characteristics of a methane hydrate-bearing soil can happen through (a) hydrate dissociation during pressure and temperature changes or (b) through soil softening due to shearing. Since methane hydrates are usually found in unconsolidated and soft formations, which are able to compact during the extraction process (see Figure 1.1), this induces changes in the stress state of the formation and consequently in the stresses of the cement and the casing of the wellbore as well. Therefore, these uncertainties could lead to potential risks during construction and production, such as soil fracture, sand production, casing damaging and cement failure [6].

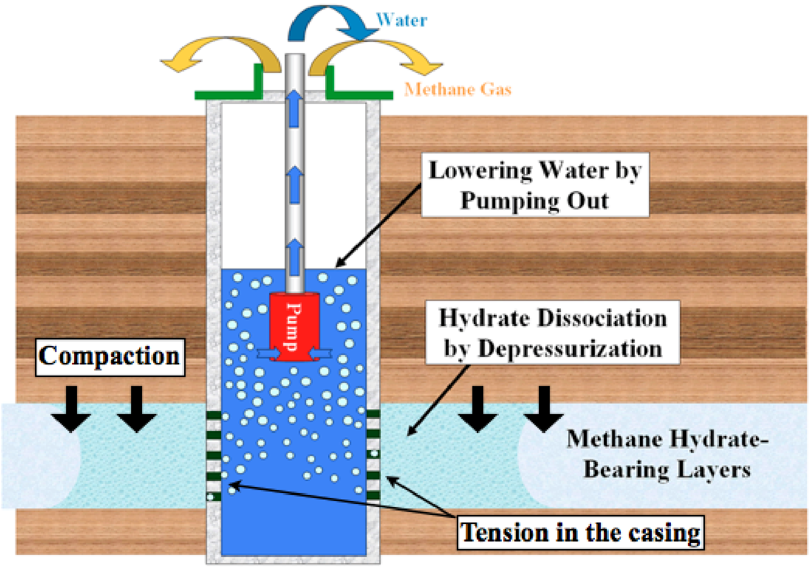


Figure 1.1: During hydrate dissociation, the formation compacts inducing tensile stresses in the casing

## 1.2 Objectives

As in any case of gas extraction, the geomechanical behaviour of the formation as well as the wellbore structural integrity and stability are serious concerns and therefore the main parameters affecting their performance need to be well understood before gas production from hydrate deposits can be further developed.

In this project, great emphasis is given to improve the understanding of wellbore behaviour during depressurization, by performing a parametric study to investigate the wellbore-formation interaction problem. Specifically, the aims of this project are to study the effect of the formation compaction profiles, the effect of the length of the wellbore and the effect of non-linear behaviour (elastoplasticity) of the casing on tensile stress induced in the casing and cracking development. Furthermore, the relationship of the tensile stresses of the casing and the formation settlement profile characteristics is to be examined. Equipped with such knowledge, one can proceed to establish design tools and guidelines for wellbore integrity and stability.

## 1.3 Scope of Research

Research began with an extensive literature review on the subject of methane hydrates and wellbore stability, to obtain background knowledge that would help to proceed with the project. The study focused on the identification of the parameters which affect the overall behaviour of a wellbore during production. Once these parameters were identified analysis were made to confirm their significance.

In order to achieve the objectives of this project, simulations were then made using a finite element model that was developed on ABAQUS by E. Xu (2014), which includes the CMHCS constitutive model [8], the effect of the construction process on the loading history and the interactions between the formation and the cement, and the cement and the casing.

A parametric study was performed by changing the parameters investigated, through the input and FORTRAN files. Data were then obtained and various analyses, evaluations and graphical representations of the data were undertaken in order to establish trends concerning the formation and wellbore behaviour during the depressurization process. Graphs were then discussed and important conclusions were established.

The conclusions of the testing and analysis of the finite element model and recommendations for further research conclude this effort.

## 1.4 Report Outline

This report contains 6 chapters, the contents of which are described below.

#### Chapter 2

This chapter initially reviews the methane hydrate geomechanical characteristics and introduces the different methods available for extracting gas from hydrates. It then discusses the geomechanical and environmental challenges faced during production. Finally, it reviews previous research relevant to investigating wellbore stability in a hydrate-bearing sediment and highlights the need for expansion of the work previously done on the parameters affecting the wellbore stability during gas production.

**Chapter 3**

This chapter describes the numerical model used to simulate the behaviour of the production trial well at the Nankai Trough in Japan. It gives the model, mesh and element dimensions and it introduces the models used for the formation (Methane Hydrate Critical State Model), cement (Mohr Coulomb Model) and casing (Elastic Model). Finally, it includes the results obtain from the numerical model during depressurization.

**Chapter 4**

This chapter describes the parametric study performed to investigate the effects of the casing length and other parameters on the formation settlement profile and casing tensile stresses. The simplified model condition and the approach and procedure followed are described. Finally, the parameters investigated in this study are listed and explained.

**Chapter 5**

This chapter presents the results obtained during the investigation of each parameter independently using diagrams which are accompanied with discussion. Furthermore, it presents the interrelationship of the tensile stresses of the casing and the formation settlement characteristics on a contour plot.

**Chapter 6**

This section concludes the findings from the work presented in this report and provides recommendations for further research.

# 2 Literature Review

## 2.1 Methane Hydrate Characteristics

Methane hydrate, otherwise known as fire ice, is a solid clathrate compound in which a large amount of methane is trapped within a crystal of ice, as shown in Figure 2.1(a). Methane, made of one carbon atom and four hydrogen atoms, is the simplest hydrocarbon molecule and the primary component of natural gas. Natural gas hydrates occur in deep oceanic sediments and to a lesser degree in permafrost regions in the arctic [9] where conditions of low temperature and high pressure exist to allow for their formation. Particularly, the earth's continental slope and rise at water depths of 500 m at low latitudes and 250 m at high latitudes may contain methane hydrate accumulations [10].

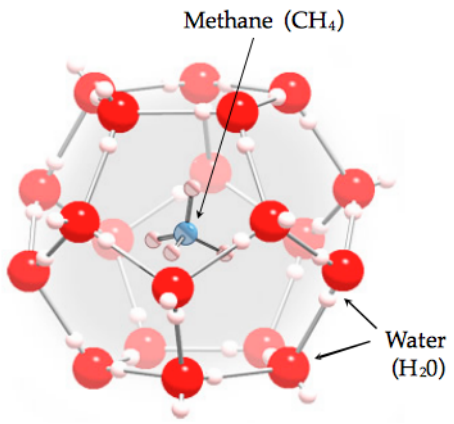


(a) Methane Hydrate Compound

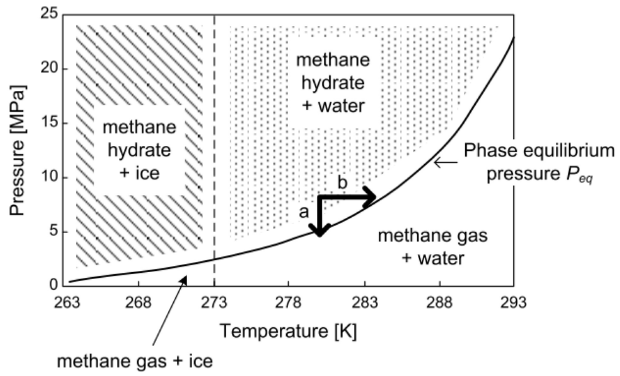


(b) Phase equilibrium curve of methane hydrate [6]

Figure 2.1: The methane hydrate compound and its characteristics

Methane hydrate soil is commonly categorized into two types based on their morphology, in relation to the location where hydrate is formed in the pore space: (a) Pore filling - hydrates exist inside the pores, resulting into a denser hydrate-bearing soil compared to that without hydrates, which is likely to act as an overconsolidated or dense soil (b) Cementing - hydrates exist at soil grain contacts and therefore, the soil is likely to behave as a bonded soil.

The mechanical characteristics of methane hydrate-bearing soil which are observed in both types of soil discussed above, are the following:

- Peak strength of hydrate-bearing soil depends on hydrate saturation ($S_h$)

- Hydrate contribution to shear behaviour is of cohesive rather than frictional nature
- Dilation angle increases with hydrate saturation
- Greater stiffness than that of soil without hydrate

In order to extract the gas, the hydrate needs to dissociate by means which change the temperature and pressure conditions into ranges where the methane hydrate becomes unstable, as shown in the phase equilibrium diagram in Figure 2.1(b). These methods include the use of a depressurization well, in which the well pressure is decreased to reduce the pressure of the surrounding soil so that methane hydrate dissociates and gas flows into the well, a thermal injection well, in which temperature is increased by injecting hot water into the well to encourage methane hydrate dissociation and the use of hydrate inhibitors, which are pumped into a reservoir to shift the hydrate phase boundary from the stability region to the dissociation region [7].

The construction operations for a production well, include conductor pipe driving, drilling, installation of casing, cementing, and cement hardening and shrinkage. Figure 2.2 (a) shows a schematic of a typical production well and Figure 2.2 (b) shows a schematic of the modelled production well.

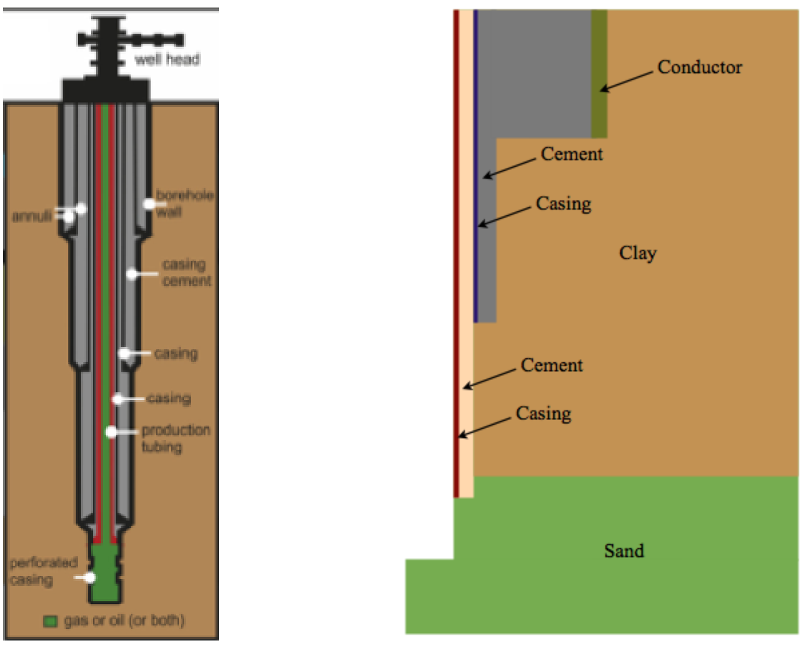


(a) (b)

Figure 2.2: Schematic of (a) typical production well [11], (b) modelled production well

## 2.2 Geomechanical Challenges

The geomechanical response of hydrate-bearing soils in general, potential well instability and casing deformation are serious concerns that need to be investigated and understood before gas production can be developed to a great extent [12]. Deposits that are identified as suitable targets for gas production usually include poorly consolidated sediments, which are often characterised by limited shear strength. Therefore, during gas production, the dissociation of the hydrates can result to a degradation of structural strength of the hydrate-bearing soil. Production induced pressure and temperature changes in the reservoir can significantly change the stress and strain state of the formation with direct consequence on the wellbore stability, the flow and fluid properties of the system, the potential for co-production of solid particles, and consequently on continuing gas production [12]. Vertical compaction, stress changes and associated strain, if sufficiently high, may initiate well instability and affect the load on the well casing [13].

Rutqvist et al.(2008) suggested that normally, reservoir compaction greater than approximately 5% appears to be a consistent indicator for potential casing failures. Casing shear is the dominant failure mechanism, typically located in the overburden up to several hundred feet above the hydrate layer. Rutqvist and Moridis (2009) [14] showed that the possibility of inducing shear failure in the reservoir depends on the initial stress field and the Poissons ratio of the formation. For example, they showed that if the stress field is initially near critical stress for shear failure, even a small pressure decrease could be sufficient to initiate shear failure in parts of the dissociated reservoir. Such shear failure may generally lead to enhance subsidence as well as sand production.

It is important to emphasize that gas hydrate dissociation takes place in the reservoir and the transition from a solid crystal to free gas and free water phases will begin next to the production wellbore, and move away over time as dissociation continues. The complexity of gas Hydrate wells arises due to some technical challenges [12], such as:

- Preserving commercial gas flows with high water production rates
- Operating with low temperatures and pressures in the wellbore, to prevent hydrate formation or freezing
- Avoiding formation sand production into the wellbore
- Ensuring well structural integrity with subsidence in the reservoir, and gas hydrate dissociation around the wellbore.

## 2.3 Environmental Challenges

Although, the amount of methane gas found in hydrate-bearing soils is enormous and it has been recognised as a potential energy resource, a crucial barrier to the utilization of this resource is the limited understanding of the gas hydrates response to production activities and the associated environmental impacts. These impacts include concerns also faced in conventional oil and gas exploration and production, such as ground subsidence related to production from shallow, unconsolidated reservoirs, land and air impacts from drilling and production activities, and disposal of produced waters [12].

Even though gas hydrates may be a major new energy resource, it has been recognised, that they probably play a major though unconstrained role to the ongoing global carbon cycling and climate changes [15]. The large amount of carbon stored in gas hydrates is likely 10 to 20 times the mass of carbon in the atmosphere. This means that a relatively small release of methane from gas hydrate systems could have significant impact. There have been also events in the geologic history were significant releases of methane from gas hydrate have likely affected global climates [16]. This probably has to do with the fact that methane is approximately 20 times more effective than $CO_2$ in terms of its overall "greenhouse effect" [17].

However, there is an intrinsic distinction between those reservoirs that could affect climate and those that are possible production sources and at this stage targeted deposits are those found in sand reservoirs that exist deeply buried in the subsurface [12] in permafrost or marine regions. As noted by Moridis et al., (2009), such deposits are closer to the gas sources, closer to the stability conditions for gas hydrate (less energy input require to dissociate them) and housed in sediments of increased mechanical integrity.

Gas hydrates are also subject to instability during environmental changes, particularly pressure and temperature. Although gas hydrates cannot exist at surface conditions, there is a concern that once the hydrate dissociates in the subsurface, it will lead to an uncontrollable "chain reaction". However, a unique feature of gas hydrates is that the hydrate transition from solid hydrate to liquid gas and free water is self-limiting. Heat is removed from the surrounding environment (endothermic reaction) thus reducing ambient temperatures and returning back to hydrate stability conditions (see Figure 2.1 (b)). Therefore, a key challenge with gas hydrate production is to keep it going, as it is anticipated that the continuous input or periodic re-application of energy inputs will be required to maintain production [18]. Moreover, it has been shown through numerical simulations of natural gas hydrate systems, that the gas hydrate dissociation reaction will naturally serve to quickly interrupt dissociation once the depressurizing perturbation is released [19]. Hence, the likelihood for gas hydrate production to result in an uncontrolled "chain reaction" is very restricted.

## 2.4 Previous Numerical Studies

Due to the fact that that the elements of the wellbore and of the surrounding formation exhibit nonlinear behaviour, and the interaction effects are dependent on multiple parameters, analytical solutions based on linear elasticity have only limited scope and reliability when used for wellbore integrity assessment. Thus research, has concentrated on numerical studies.

Salehabadi et al. (2008) [20] studied the interaction between the cement, casing and the surrounding formation including the debonding effect. They developed a numerical model in order to study the effect of variable formation conditions to the stress state of the wellbore without considering material non linearity and/or the construction sequence.

Rutqvist et al. (2012)[21], conducted numerical analysis of the thermal and geomechanical processes during gas production to study wellbore stability using a purpose made simulator within the $FLAC^{3D}$ processor. The well casing membrane, bending and frictional properties were modeled and the behaviour of the formation was modeled using a Mohr-Coulomb shear failure criterion. The study considered the effects of fluid and thermal flow to the formation but not the effects of formation behaviour to the wellbore.

Klar et al. (2010) [22], Kimoto et al. (2010) [23], and Kim et al. [24] (2012), also used numerical analysis in order to study the behaviour of methane hydrate bearing sediments during depressurization. However, their analysis codes do not incorporate the hydrate dissociation effect on the mechanical behaviour of the formation and only one (Kimoto et al., 2010) includes the thermal effect.

Uchida et al., (2012) [8], developed the Cambridge Methane Hydrate Critical State model (CMHCS) that incorporates all of the important parameters in wellbore formation interaction, namely, volumetric yielding, enhanced cohesion, dilation and stiffness from the presence of the hydrate, strain softening due to shearing deformation and degradation of hydrate cementing and interlocking by plastic straining. This model has proven to more reliably simulate experimental and case study data (Masui et al., 2006, E. Xu, 2014).

E. Xu, (2014), investigated the wellbore behaviour during methane gas recovery from hydrate bearing sediments using numerical analysis. He used CMHGS to simulate the depressurization process, along with the resulting effects of hydrate dissociation and the changes in pore water pressure over time and to study their effects on the casing. A parametric study was then undertaken focusing on the effects of the friction coefficient, the cement stiffness and the wellbore length and the formation compaction profile on the behaviour of the wellbore casing. He highlighted that the settlement profile of the soil would affect the stress state of the casing but he concluded that more work should be done in order to confirm this suggestion.

The study by Ermao Xu, constitutes the basis for the investigation presented herein and it is therefore further examined in the next Chapter.

## 2.5 Summary of Literature Review

The literature review demonstrated that there have been only few numerical studies on the formation-wellbore interaction problem and most studies have concentrated on the thermal and hydro effects of the wellbore to the formation and provide limited and inconclusive results on the effects of the formation behaviour to the wellbore.

It was also established that the most notable previous numerical studies have used constitutive models that do not include the hydrate dissociation effect. This effect was incorporated in the study by E. Xu (2014) and was found to provide a better approximation to experimental and case study data.

Although the results in the previous study have demonstrated the possible effects of the formation compaction profiles on casing stress state, they were not conclusive as to the interrelationship between compaction profile and casing behaviour nor to the geotechnical parameters of the formation that affect the profiles, or to the parameters of the wellbore (length, elasto-plastic behaviour) that influence casing stress development and overall behaviour.

Thus the parametric study described herein is undertaken in order to provide further insight to the formation - wellbore interaction problem.

# 3 Computational Model Validation

This chapter presents a finite element model that was developed by E. Xu (2014) on ABAQUS which includes the constitutive model specifically developed for methane hydrate-bearing soils (MHCS), the effect of the construction process on the loading history and the interactions between the formation and the cement, and the cement and the casing. The model computes the stress state of the wellbore at each construction and production stage and the results are compared with the experimental results taken from the production trial Well at Nankai Trough.

During the extraction process, once the hydrate dissociates either through a decrease or increase in pore pressure or in temperature, the hydrates inside the pores disappear and the soil may behave as a less dense soil or as an unbonded soil [25]. This produced the need of a new constitutive model which incorporates the effect of hydrate on the stress-strain behaviour of soils, the Methane Hydrate Critical State model (MHCS).

## 3.1 Case Study - Production Trial Well, Nankai Trough, Japan

To prove the feasibility of depressurization method for producing methane from hydrates in deepwater sediments, Japan Oil, Gas, and Metals National Corporation (JOGMEC) conducted the wellbore stability study of the production trial well in the Nankai Trough in Japan, in March 2013. This is one of the limited field studies available concerning methane hydrate-bearing soils. The site was selected based on seismic and well data collected from 2001-2008 that indicate methane hydrate-rich sedimentary layers in this area and is shown in Figure 3.1. The field program included drilling a production well and two monitoring wells, acquiring extensive downhole data including pressure core samples and carrying out a production flow test [26].

In that area, the water depth is 1010 m, the whole length of the well is 319 m and the hydrate-bearing sediments are found to be 270 m below the seabed within coarse-grained sediments [7].

From this trial well, JOGMEC managed to extract methane gas from the hydrate-bearing sediments by the depressurization method. The bottom hole pressure decreased by 10MPa on average and approximately 120, 000 cubic meters of methane gas were produced totally. However, the production had to be terminated a few days later after an increase in sand production occurred [27].

Furthermore, investigations about the stress state of the formation, cement and casing

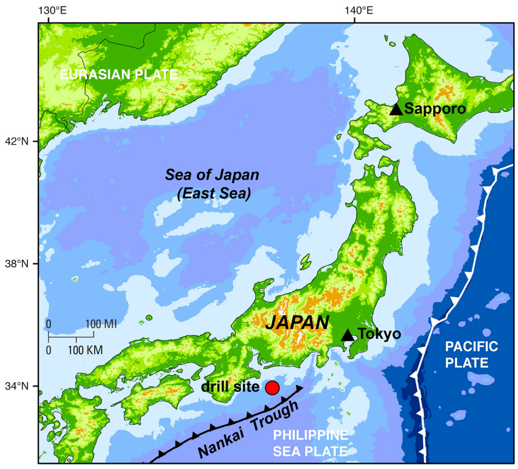


Figure 3.1: Nankai Trough methane hydrate in Japan

were carried out. It was found that, during construction, the vertical stresses and pore water pressure did not change significantly. During production though, they did change and it was observed that the hydrate saturation and pore pressure in the formation decreased, and the reduction propagated outwards, inducing significant compaction.

This indicates the importance of evaluation of the state of wellbore in order to produce methane gas safely and efficiently avoiding any unwanted consequences. Hence, there is obviously the need, to be able to predict the stress changes and plastic strain evolution of the wellbore during the lifetime of the well [6].

## 3.2 Finite Element Wellbore Model of Case Study

In this section, the finite element wellbore model, specifically designed for methane gas production to simulate the construction and operations of the production well and the interaction between cement-casing-formation is described. The dimensions of the model are described, as well as the material properties used and finally the results obtained during depressurization and the effects of the stress changes in the formation on wellbore stability during production are examined.

### 3.2.1 Model Dimensioning

A 2D analysis was performed with axisymmetric conditions because of the symmetry of the problem. The ABAQUS finite element model, shown in Figure 3.2 below, has an outer radial distance of 300m in order to avoid the boundary effect in the production process. The length of the wellbore, which includes the conductor, casing, cement and liner, is 320m and the vertical dimension of the model is 360m covering the whole length of the wellbore.

A fine mesh was concentrated near the wellbore region, ranging from 0.0046m radial width at the wellbore to 24.36m at the outer boundary, to make the model more computationally efficient (see Figure 3.2). The mesh size at the methane hydrate-bearing layer was very fine as well in order to consider the effect of fine soil layering and hydrate heterogeneity, observations of the Nankai Trough site. Moreover, the formation model was composed by 70,200 axisymmetric elements and 212,205 nodes [7].

Two differenet element types were applied in the model, both axisymmetric. CAX8 (8-node element shown in Figure 3.2) was used for the conductor, liner, casing and cement and CAX8P for the formation and gravel elements as this type considers the pore pressure [7].

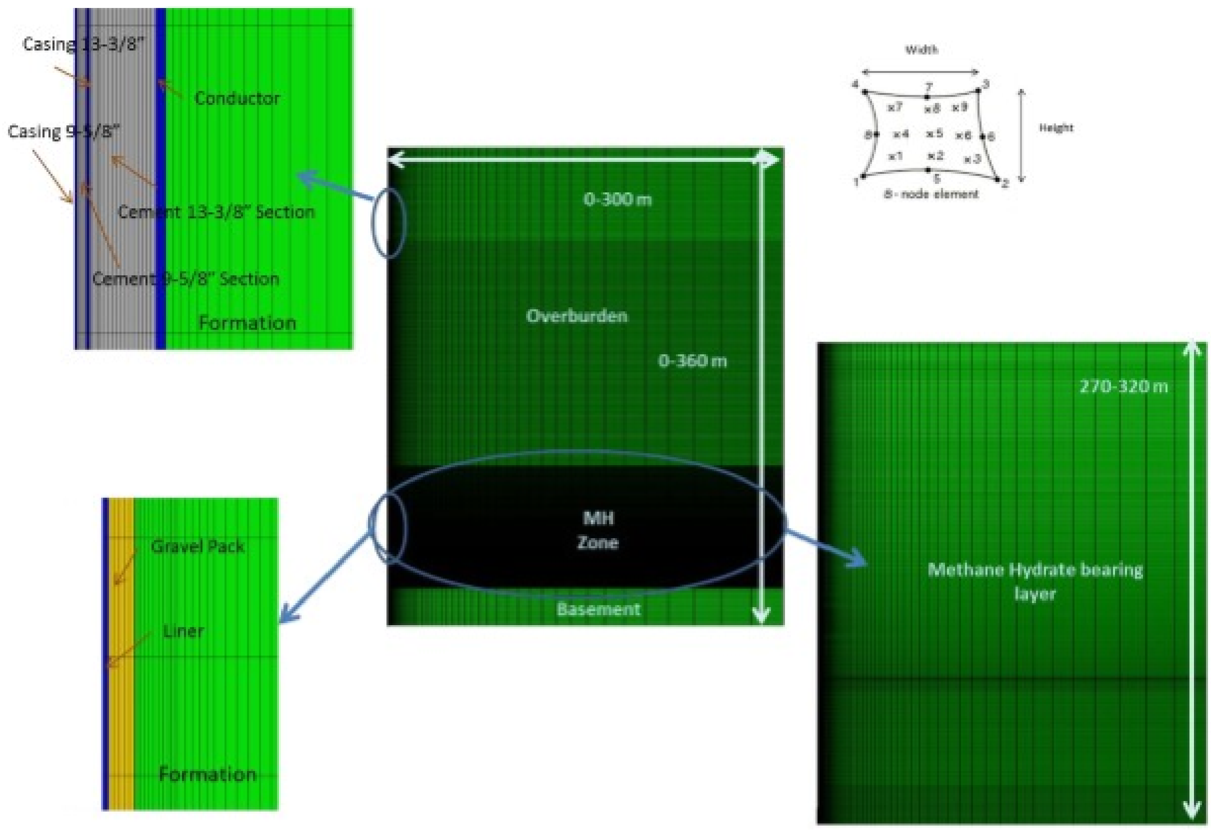


Figure 3.2: ABAQUS finite element mesh of the production well model [7]

### 3.2.2 Material Properties

**Methane Hydrate Critical State Model**

A fully-coupled thermo-hydro-mechanical formulation (MHCS) for hydrate bearing sediments was developed at Cambridge to simulate the fluid, thermal and mechanical behaviour of hydrate bearing sediments in a coupled manner, as discussed in [8]. This model is a simple extension to the critical state model. Both models can describe the strength, compression and dilatancy as well as the critical state at which the soil can have unlimited distortion without any changes in volume or stress.

Figure 3.3, shows the volumetric yielding that can be captured by a critical state model under isotropic loading. It can be seen that the soil becomes fully plastic when the mean effective stress $p^{'}$ reaches the volumetric yiled stress $p^{'}_{cs}$ and the response changes from a gradient $\kappa$ to a steeper gradient $\lambda$. Generally, $\kappa$ represents the slope of the line in v:ln $p^{'}$ while the soil is still elastic (swelling line), whereas $\lambda$ represents the slope of the line while the soil is plastic (compression line).

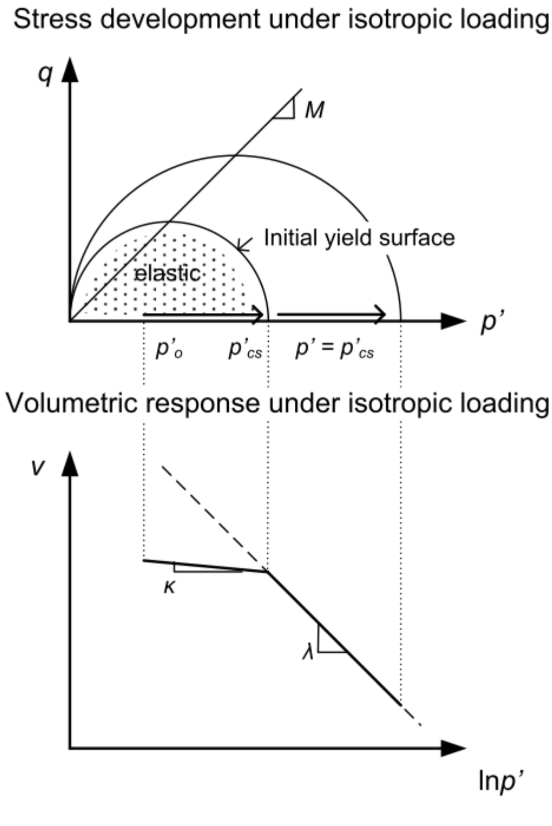


Figure 3.3: Yield surface and volumetric response in critical state models [8]

The MHCS model introduces five extra model parameters to the conventional critical state model in order to represent features which make the methane hydrate bearing soils to differ from other soils. These include: (1) enhanced cohesion, stiffness, strength and dilatancy, (2) volumetric yielding, which plays an important role when the hydrate soil undergoes a significant change in effective stresses and hydrate saturation during depressurization, (3) strain softening due to shearing deformation, (4) smooth nonlinear stress-strain relationship and (5) degradation of hydrate cementing. Such behaviour at large strains may be important for wellbore stability.

Figure 3.4, shows the yield surface of MHCS model which includes both cohesion enhancement - enlargement of yield surface uniformly on both sides of the original yield surface (see Figure 3.3) and dilation enhancement - greater normal angle to the tangent of the surface when the soil yields at a given mean effective stress $p'$ at the dry side of the critical state (yield surface expands to the right hand side of the original yield surface). The parameters $p'_{cc}$ and $p'_{cd}$ shown in the figure below, are the additional hardening parameters associated with cohesion and dilation respectively [8].

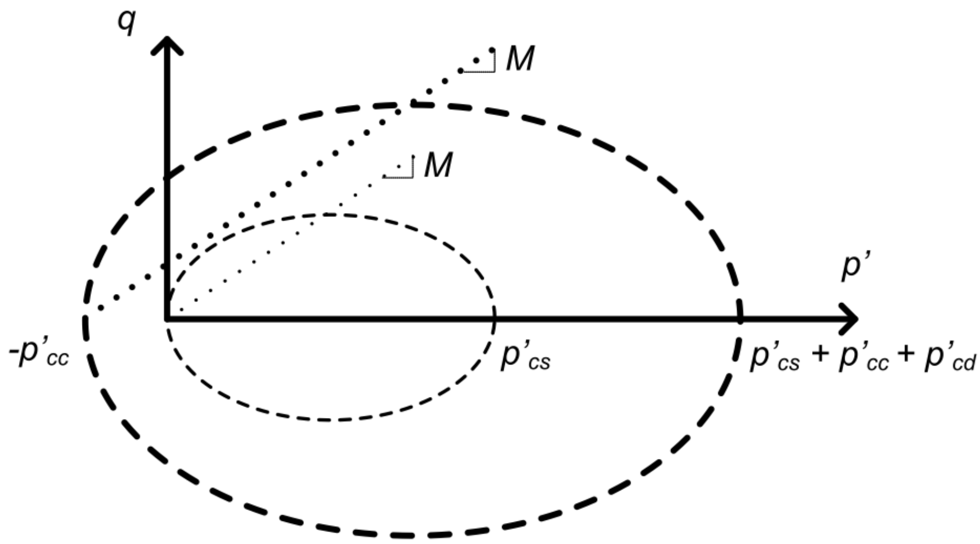


Figure 3.4: Yield surface of MHCS model with enhanced cohesion and dilation [8]

The material properties of clay and sand used in the model were determined based on laboratory results on recovered soil core samples from Nankai, Trough in Japan. The Methane Hydrate Critical State model was used for both the clay rich layer and the sand rich layer (hydrate bearing soil). The mechanical behaviour of the clay was modeled with zero hydrate saturation conditions. Table 1 below, summarizes the soil properties used in the model for both the clay rich and sand rich layers. Critical state line, M, normal compression line, $\lambda$ and swelling line, $\kappa$ are the conventional critical state parameters. Parameters (a, b, c, d, m, $m_2$ and U) [28] were used to calculate the hydrate dependent parameters, such as additional hardening parameters for cohesion, $p_{cc'}$, for dilation $p_{cd'}$ and elastic shear stiffness.

Table 1: Mechanical properties used in the formation

| Parameter | Clay | Sand |
|---|---|---|
| Swelling parameter ($\kappa$) | 0.008 | 0.007 |
| Compression parameter ($\lambda$) | 0.2 | 0.3 |
| Critical state ratio ($M$) | 1.46 | 1.37 |
| Porosity ($n$) | 0.54 | 0.54 |
| Poisson's ratio ($\nu$) | 0.35 | 0.35 |
| $a$ | 50000 | 50000 |
| $b$ | 2.1 | 2.1 |
| $c$ | 400 | 400 |
| $d$ | 2 | 2 |
| $m$ | 0.1 | 0.1 |
| $U$ | 10 | 50 |
| $m_2$ | 200000 | 200000 |

### Cement and Casing Models

The ABAQUS built-in Mohr Coulomb model was used for cement modeling and the casing was assumed to be elastic [7].

Table 2 summarizes the material properties for the cement and the casing of the production well.

Table 2: Mechanical properties used in the cement and the casing

| Parameter | Value |
| --- | --- |
| **Cement Mohr Coulomb Model** | |
| Density ($\rho$) (kg/$m^3$) | 1240 |
| Young's modulus (E) (Slurry) [MPa] | 132 |
| Poisson's ratio ($\nu$) (Slurry) | 0.49 |
| Young's modulus (E) (Solid) [MPa] | 3810 |
| Poisson's ratio ($\nu$) (Solid) | 0.21 |
| Cohesion (c) [kPa] | 9170 |
| Friction angle $\Phi$ | 0 |
| Dilation angle $\psi$ | 0 |
| Shrinkage ratio | 0.1% |
| Shear Strength [kPa] | 9411 |
| **Casing Elastic Model** | |
| Density ($\rho$) (kg/$m^3$) | 8000 |
| Young's modulus (E) [GPa] | 200 |
| Poisson's ratio ($\nu$) | 0.27 |

### 3.2.3 Results Obtained During Depressurization

For the production model, the stress and deformation state of the well obtained during its construction, are used as the initial conditions for the production stage. During depressurization, the pore pressure was designed to decrease linearly by 10MPa by the end of the depressurization period, as shown in Figure 3.5.

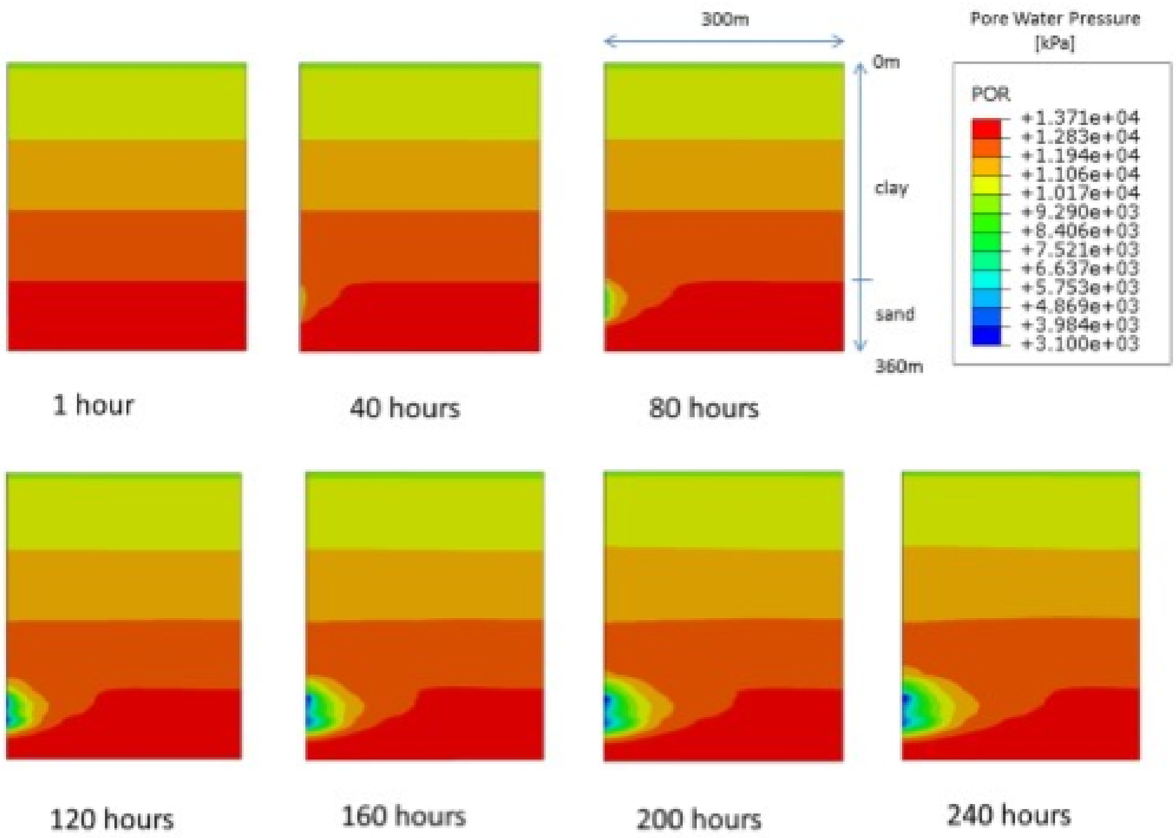


Figure 3.5: Pore pressure [kPa] at 0, 40, 80, 120, 160, 200 and 240 hours during the production trial at Nankai Trough [7]

The effects of the depressurization on the stress and strain developments are the following [7]:

- Depressurization resulted into an increase of the effective stress due to the reduction of the pore pressure and this in turn led to a compressive deformation and volumetric yielding of the hydrate sediment.
- Due to hydrate dissociation, plastic strain developed near the wellbore and significant stress relaxation caused the stress to be transferred to stiffer hydrate sediments, thus increasing the effective stress particularly in the vertical direction.
- Soil arching developed at the interface of the clay rich and sand rich layers inducing stress variations in the casing through the cement.

- During depressurization, the results showed that radial and circumferential stresses of the casing were unchanged. However, a high tensile stress was developed at the bottom of the casing as shown in Figure 3.6, due to the compaction of the soil below. This was because the casing was supported by the higher layers, but was dragging downwards at the bottom.

- The cement showed a similar behaviour to the casing. However, the vertical stresses of the cement reduced because of the compaction of the soil below, dragging the cement downwards, but it was shown that they where still in compression.

This shows the potential risk of the casing failing in tension, therefore a parametric study is performed to examine the factors influencing the behaviour of the casing due to compaction of the soil below.

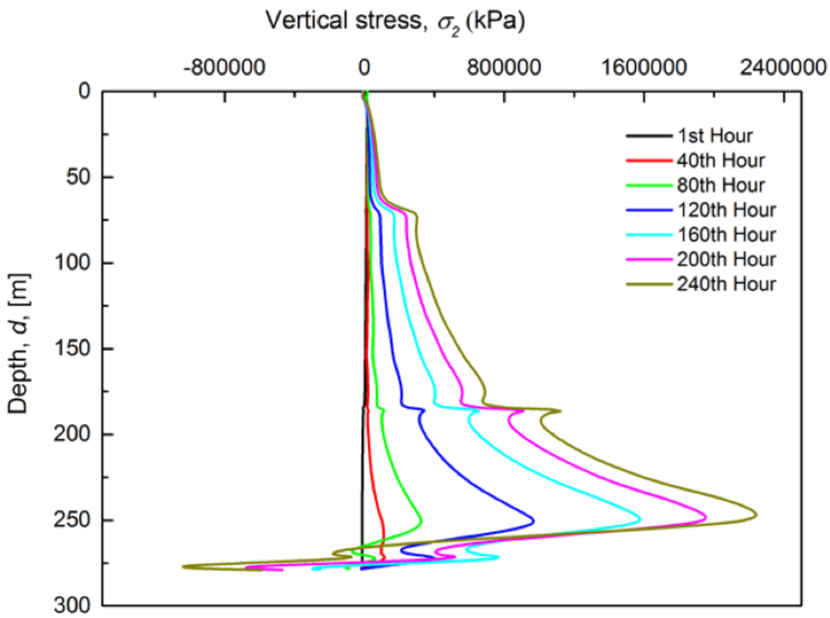


Figure 3.6: Vertical casing stress at 0, 40, 80, 120, 160, 200 and 240 hours at the inner site during gas production trial at Nankai Trough site in Japan [7]

# 4 Computational Parametric Study

In the case of depressurization which is the technique investigated herein, it is anticipated that soils characterised by low pre-consolidation pressures, where depressurization would increase the mean effective stress to the extent that their pre-consolidation pressure would be exceeded, would undergo considerable compaction particularly in the vicinity of the wellbore affecting wellbore structural integrity and stability. The parameters affecting the compaction process and the associated wellbore interaction effects have not been sufficiently investigated and/or understood to date and further studies are required [7], [12].

Therefore, a parametric study is performed, in order to investigate the behaviour of the wellbore casing in the vertical direction during depressurization. Potential parameters affecting its behaviour are (a) friction coefficient between the cement and the casing, (b) cement stiffness, (c) casing length and (d) formation settlement profile. Previous studies *(E. Xu, 2014)* [7] have shown that the friction coefficient between the cement and the casing and the cement stiffness are not very important factors that govern the magnitude of the tensile stress induced in the casing. Therefore, casing length and parameters affecting the formation settlement profile and casing tensile stresses are further investigated in a systematic manner, in order to confirm previous findings and to produce more data that would provide further insight to the geomechanical behaviour of the formation and its interaction with the wellbore casing.

## 4.1 Model Condition

The ABAQUS model mentioned earlier is used, but several wellbore components (such as conductor pipe, liner etc.) are eliminated to increase the computational efficiency of the simulation and to simplify it. The study mainly focuses on a wellbore of 300m length (indicated as $L$ in Figure 4.1), with the depressurization zone extending 50 m (indicated as $d$) below the bottom of the casing (e.g. 300-350 m from the top of the model) as shown in Figure 4.1 below. The model has a vertical dimension of 400m and a horizontal dimension of 300m to avoid any boundary effects. The pressure is reduced at the inner side of the depressurization zone and the reduction in pore pressure propagates outwards, in the direction of $R$, as shown in Figure 4.1. A uniform water pressure of 10,100 kPa is applied on the top of the model as well as the in situ stress of the formation.

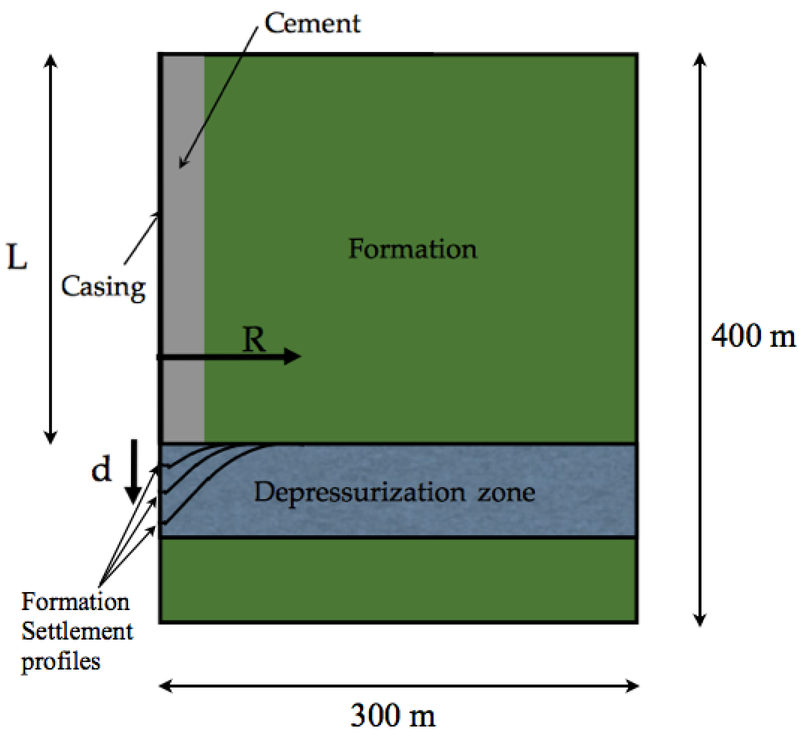


Figure 4.1: Simple ABAQUS model representation

## 4.2 Approach and Procedure

As suggested earlier, the compaction of the soil was the main depressurization effect related to stress changes in the casing that required further investigation. Therefore, in this study, different pore pressure reduction profiles are considered, in order to improve the understanding with respect to formation settlement and casing tensile stresses during depressurization. For each simulation the distance to which the pore pressure propagates outwards from the centreline of the wellbore, $R_i$, is fixed, for example $R_i = 30m$. The pore pressure is then reduced in steps and linearly between the steps to make the model more computationally efficient. For example, in every time step the pore pressure reduces by 1000 kPa in every 3 m distance (chosen to be $R_i/10$) radially outwards from the centreline of the wellbore.

The geometry of the formation settlement profile is shown in Figure 4.2 below, where $S_{max}$ is the maximum settlement of the wellbore and $i$ is the distance from the axis to the point of inflection (trough width). It can be seen, that the maximum settlement occurs at the near-wellbore region and the settlement reduces as the radius increases outwards.

By changing both $S_{max}$ and i, different formation settlement profiles are formed, but those of interest are the ones with small values of i and large values of $S_{max}$, as these are expected to produce the maximum differential settlements between adjacent elements in the model, and hence the highest tensile stresses in the casing.

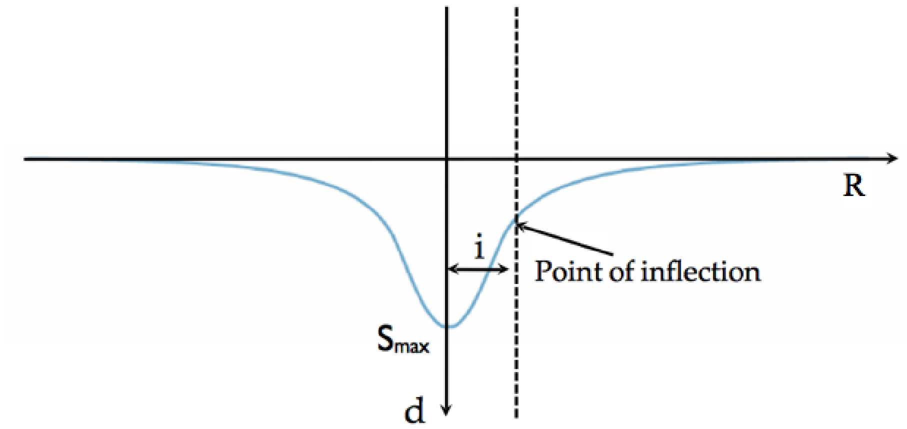


Figure 4.2: Formation settlement profile

## 4.3 Investigated Parameters

The parameters investigated in this study are the following:

- Distance to which pore pressure propagates ($R_i$)
- Elasto-plasticity of the casing
- Length of the wellbore ($L$)
- Soil compression characteristics (swelling ($\kappa$) and compression ($\lambda$) parameters)

The effects considered for each parameter varied include the following:

- Formation compaction profiles (characterised by $S_{max}$ and $i$)
- Tensile stress in the casing ($\sigma$)

Distance of Pore Pressure Reduction:

To look into the effect of the distance of pore pressure reduction, $R_i$ has been varied from 10-100 (i.e. 10, 15, 20, 25, 30, 40, 100). Its effect was considered on the formation compaction profiles and the tensile stress in the casing. Cases of smaller $R_i$ were preferred though, as for very large values of $R_i$, the pore pressure reduction, $\Delta$u, propagates outwards a very long distance, resulting into a uniform compaction throughout, which is thought not to be critical. Differential settlements at the near-wellbore region are thought to be more likely to cause significant changes in the stress state of the casing.

Elasto-plasticity of the Casing:

The stiffness of the casing was modeled as an elastic material of infinite tensile strength, and a Young's modulus (E) of $200GPa$ and a Poisson's ratio of 0.27, for all the previous analysis made by E. Xu (2014). This was probably too conservative and was decided to be changed to an elasto-plastic material to investigate the effect on the formation settlement profiles and the tensile stresses induced in the casing. It was assumed to give more accurate results of stress in the plastic range, as in reality the casing cannot be fully elastic.

ABAQUS requires yield stress and plastic strains of the material in the plastic range to be manually loaded into the material properties [29]. Therefore, for an elastic-perfectly plastic material the yield stress at a zero plastic strain needs to be defined as well as other points in order to create the curve of stress vs strain. A simple representation of the actual stress vs strain curve was used in this case, which includes two straight lines, one representing the elastic region and one the plastic region, as shown below in Figure 4.3. Plastic strains are calculated by subtracting the elastic strain at each point on the stress-strain curve, hence for the graph shown below, the plastic strain for $\sigma$ = 400 kPa is $\epsilon_p = 0.0$ and for $\sigma$ = 600 kPa is $\epsilon_p$= 0.2.

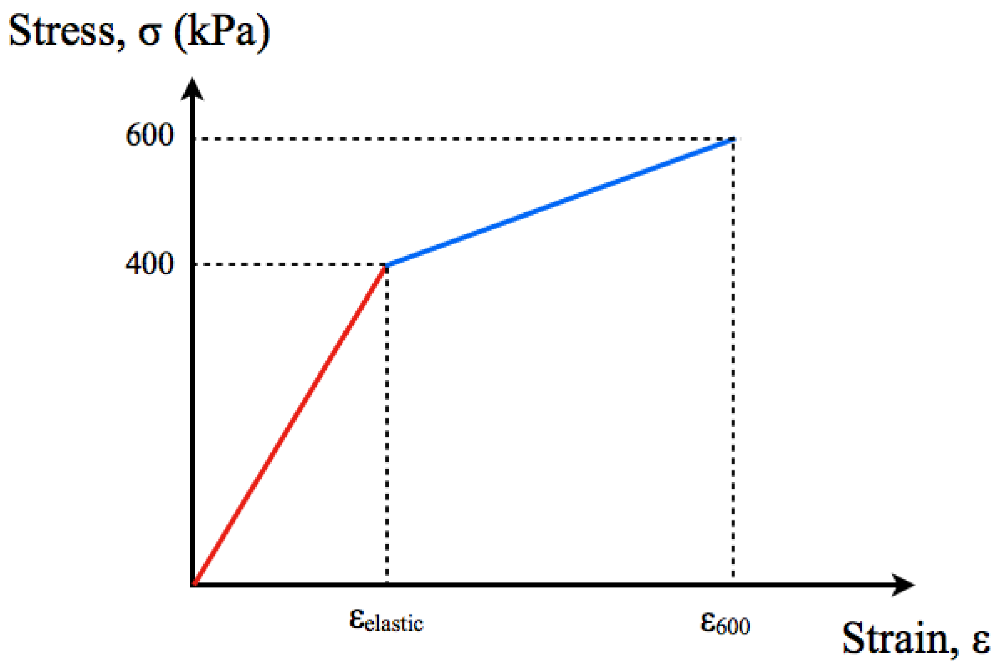


Figure 4.3: Simple representation of a stress-strain graph of an elasto-plastic material

Length of the Wellbore:

For the investigation of the length of the casing, two different cases are performed for $L = 100m$ and $L = 300m$. For each case of $L$, the value of $R_i$ has been varied such as $R_i = 30, 40, 50$.

Soil Compression Characteristics:

Initially, the soil swelling and compression parameters used, were extracted from the test data obtained from the hydrate-bearing sediments at the Nankai Trough in Japan.

For the results presented in the next chapter, the following parameters were initially fixed during the simulations with values as shown in Table 3. Refer to section 3.2.2 for the meaning of each parameter.

Table 3: Mechanical properties for the methane hydrate critical state model

| Parameter | Value |
|---|---|
| Swelling parameter ($\kappa$) | 0.05 |
| Compression parameter ($\lambda$) | 0.2 |
| Critical state ratio (M) | 1.46 |
| Porosity (n) | 0.54 |
| Poisson's ratio ($\nu$) | 0.35 |
| $a$ | 50000 |
| $b$ | 2.1 |
| $c$ | 400 |
| $d$ | 2 |
| $m$ | 0.1 |
| $U$ | 10 |
| $m_2$ | 200000 |

However, these were then varied in order to investigate their effect on the formation compaction profiles and the tensile stresses in the casing. Three different values for both the swelling ($\kappa$) and the compression($\lambda$) parameters, were chosen such as to cover a wide range of possible values.

In order to form settlement profiles with small values of $i$ and large values of $S_{max}$, which are the most critical cases, the stiffness of the soil (characterised by $\kappa$ and $\lambda$, see section 2.2) as well as the amount of pore pressure reduction and the distance of pore pressure reduction ($R_i$), were varied to find the ones causing the greatest settlements and tensile stresses in the casing. Simulations were run on ABAQUS varying each parameter one at a time in order to investigate their effect independently. The results of all of the simulations done are presented and discussed in the next chapter.

# 5 Results and Discussion

Due to depressurization, compaction of the surrounding formation takes place leading to downward movement of the cement and the casing. In general, closer to the depressurization zone, the downward movement of the formation is more than that of the cement and of the casing, resulting in the development of incremental tensile stresses within the casing. On the other hand, at shallower depths, where the depressurization effect is small, the casing settles more than the formation causing an incremental compressive stress into the casing.

Frictional stresses developing at the interface between formation and cement and between cement and the casing depend upon the incremental relative displacements between these components.

The parameters listed in section 4.3 are all investigated separately and their effect on both the formation compaction profiles and the tensile stress in the casing is discussed.

## 5.1 Distance of Pore Pressure Reduction $R_i$

Different settlement profiles were produced by assigning different pore pressure profiles within the formation, resulting in different amounts of consolidation. The distance of pore pressure reduction, $R_i$, was varied and its effect on the formation compaction profiles and on the tensile stresses induced in the casing was examined. Values of $R_i$ used were 10, 15, 20, 25, 30, 40 and 100m.

### 5.1.1 Effect on Settlement Profiles

The different formation settlement profiles were used in order to evaluate their effect on the stress state of the casing during the depressurization process. For each value of L and $R_i$, a formation settlement profile was plotted and its characteristics $S_{max}$ and i (see section 3.2) where found. Figure 5.1 below, shows the case of $L = 300m$.

It can be seen, that as $R_i$ increases, $S_{max}$ and i also increase but the gradient of the curve becomes less and less steep. Although the case of $R_i = 100$ might look like the worst case scenario as $S_{max}$ is the largest, this is not the case, as critical are considered those combinations of $S_{max}$ and i, which induce differential settlements in the formation. These are induced with a combination of small values of i and large values of $S_{max}$. On the other hand, those combinations that induce high $S_{max}$ but with less steep gradients

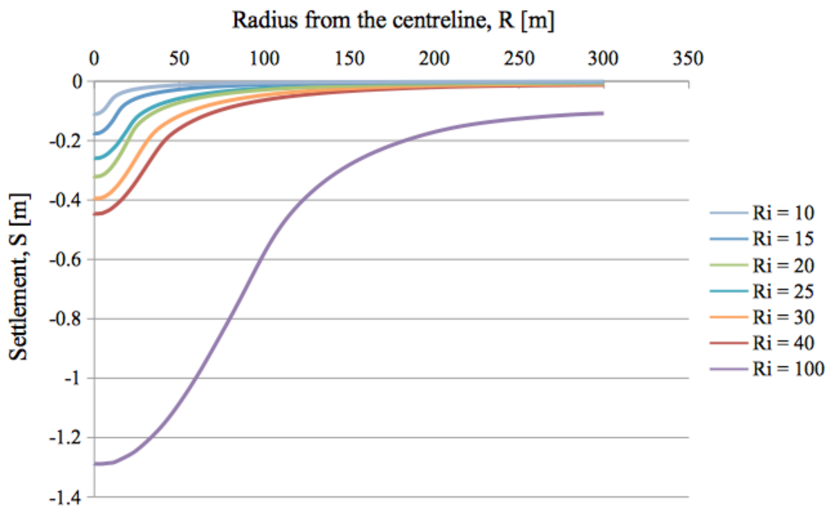


Figure 5.1: Formation settlement profiles for $L = 300m$

(larger values of i), result into a uniform compaction throughout, which is not the most critical case, as the wellbore will settle uniformly like a rigid body. Similar results are found for the case of $L = 100$m.

### 5.1.2 Effect on Tensile Stresses in the Casing

From the computational results, as it can be seen in Figure 5.2 (a), it was found that the maximum tensile stress induced in the casing is at a small distance above the bottom of the casing. This is the case for all the analysis of different $R_i$. For the case of $L = 300m$ this maximum tensile stress, was found around $280m$ depth.

This result is not straightforward, but suggests that most of the under pressure dissipation occurs in the region close to the bottom of the wellbore and therefore most of the differential settlement of the formation occurs in this region. This differential settlement is transferred by friction as a differential elongation and causes the maximum tensile stress. The maximum tensile stress occurs, at the point where the sign of the relative movement between the formation and the casing changes (i.e zero relative movement), as shown in Figure 5.2 (b).

The shape of the curve confirms the vertical tensile stress profile obtained by E. Xu (2014), shown in Figure 3.6 earlier in section 3.2.3.

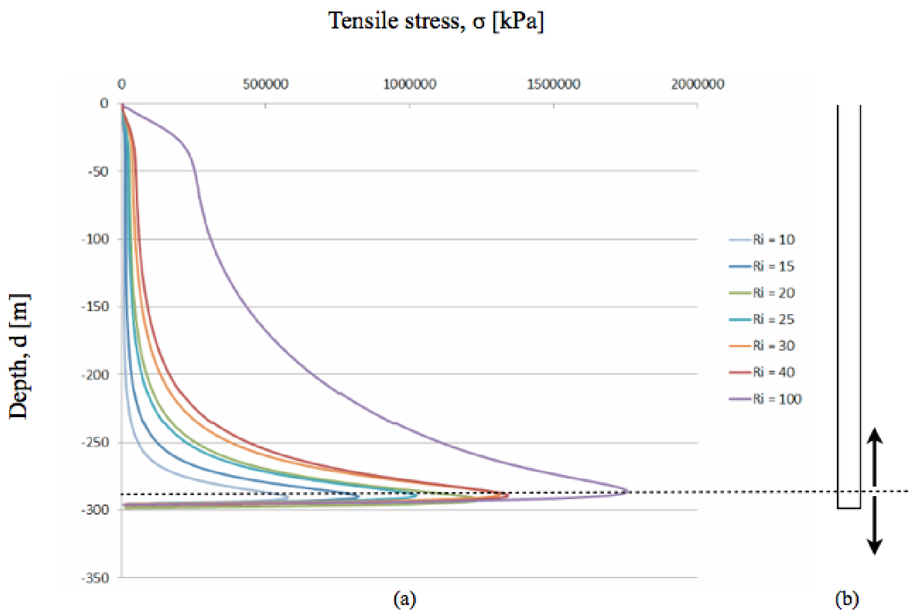


Figure 5.2: (a) Tensile stresses induced in an elastic casing for $L = 300m$, (b) Formation settlement relative to wellbore

## 5.2 Elasto-plasticity of the Casing

Once the model was changed to elasto-plastic, the effect of this change on the tensile stresses induced in the casing was examined. Figure 5.3 below shows that the maximum tensile stress induced along the length of the wellbore for all different values of $R_i$ is found to be around 400 MPa, as expected.

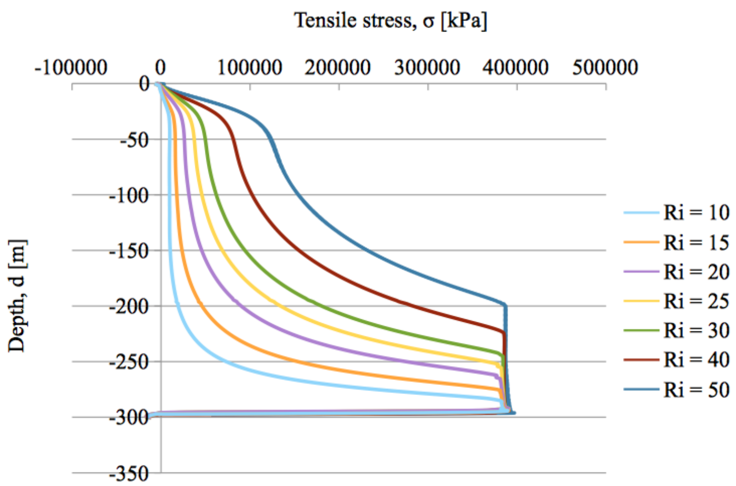


Figure 5.3: Tensile stresses induced in an elastoplastic casing for $L = 300m$

It can be seen that the curves follow the same shape as the ones produced for the casing being elastic (Figure 5.2) until the point the tensile stress reaches its maximum value ∼ 400 MPa. The corresponding value of this point on the y-axis extracted from the total length of the wellbore, shows the depth of the casing which has entered the plastic region. Therefore, it can be seen that as the distance of pore pressure reduction ($R_i$) increases, the depth of the plastic region also increases.

It can be concluded that the elastic model for the casing was unrealistic, resulting in excessive amount of tensile stresses. Therefore, the elasto-plastic model for the casing was used for the rest of the study and analysis overtaken, as it was found to represent better the actual behaviour of the wellbore during depressurization.

## 5.3 Length of the Wellbore

In this section, two different lengths for the wellbore, $L = 100$m and $L = 300$m, were chosen to be analysed. Their effect on the maximum settlements and on the tensile stresses induced in the casing is examined and compared.

### 5.3.1 Effect on Settlement Profile

Figure 5.4 shows the maximum settlements for varying values of $R_i$ for a wellbore of 100$m$ length. The shape of the graph has the same form as the one of length $L = 300$m (see Figure 5.5), but the maximum settlements are greater than those for the case of $L = 300$m. For example, for $R_i = 40$m and $L = 300$m the maximum settlement is 0.67m whereas for $L = 100$m, the maximum settlement is 1.88m.

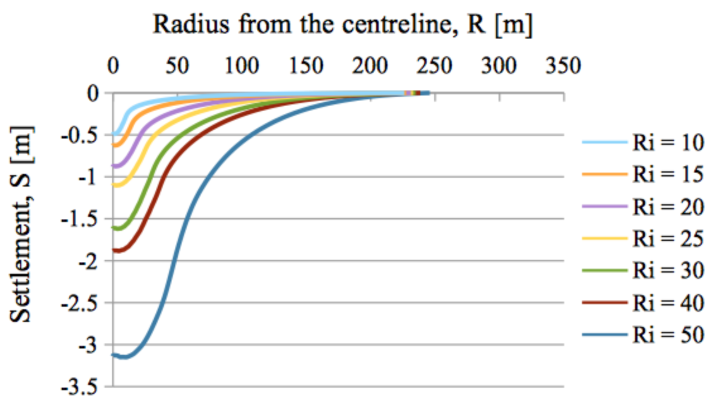


Figure 5.4: Settlement profile for 100m wellbore

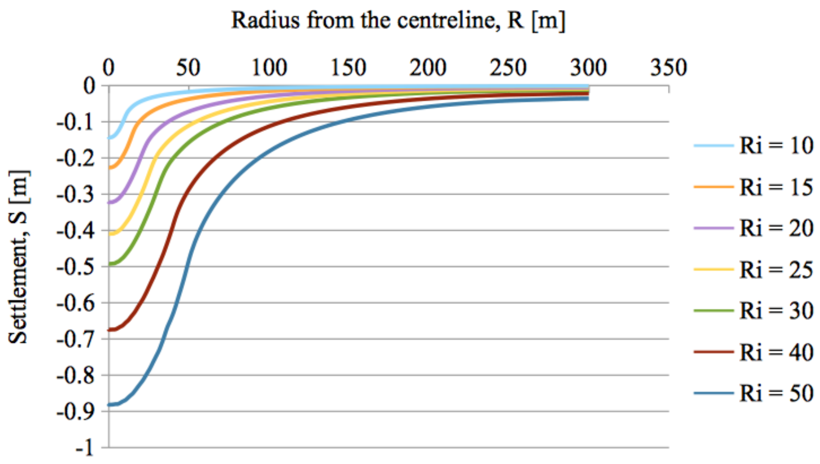


Figure 5.5: Settlement profile for 300m wellbore

This is an interesting result showing that as the length increases the wellbore is found in deeper soil which is much stiffer than the case of a shorter wellbore because of the increased overburden pressure. Since the amount of depressurization is the same for both cases, the effective stress must be greater for a wellbore of $L = 300$m than that for $L = 100$m. In the critical state models, the stress-dependent elastic soil bulk modulus $K^{'}$ is given by [30]

$$K^{'} = \frac{\nu}{\kappa} p^{'} \tag{5.1}$$

where $\nu$ is the specific volume defined as $(1+e)$, $\kappa$ is the slope of a swelling line and $p^{'}$ is the mean effective stress defined as compression positive. Therefore, as $p^{'}$ is greater for a wellbore of 300m length than that of 100m, $K^{'}$ is also greater, giving a stiffer formation. Apart from greater settlements, it can also be seen that the trough width is less in the case of $L = 100$m than that of $L = 300$m, giving more severe results.

However, in order to compare the results better, settlements of the same magnitude, for the same $R_i$ must be used. To obtain these kind of settlements, it was decided to reduce the pore pressure reduction of $L = 100$m accordinlgy, in order to give the desirable data.

Figure 5.6 below shows the settlement profiles for a wellbore of $L = 100$m where the maximum settlements for each value of $R_i$ are approximately the same with those for $L = 300$m and should be compared with Figure 5.5. The values of $R_i$ used to compare the results, are $R_i = 20, 30, 40, 50$. The trough widths of these profiles are very similar, but in order to have a better comparison, the formation profile characteristics for these two different wellbore lengths are summarized below in Table 4. It can be seen that for similar maximum settlements the trough widths of the settlement profiles are also very similar. This result leads us to the conclusion that the length of the wellbore has no effect on the formation settlement profiles when the maximum settlement is the same for all lengths of the wellbore.

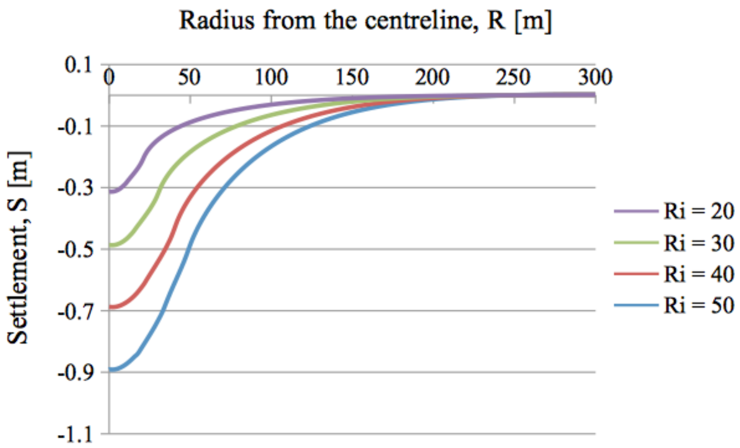


Figure 5.6: Formation settlement profile for an elastoplastic casing

Table 4: Formation profile characteristics for $R_i = 40$m

| $R_i$ [m] | $L$ [m] | $S_{max}$ [m] | $i$ [m] |
|---|---|---|---|
| 20 | 100 | 0.31314 | 20.698 |
| 20 | 300 | 0.32169 | 20.672 |
| 30 | 100 | 0.48672 | 30.179 |
| 30 | 300 | 0.49180 | 30.133 |
| 40 | 100 | 0.68759 | 40.016 |
| 40 | 300 | 0.67352 | 39.949 |
| 50 | 100 | 0.89138 | 48.293 |
| 50 | 300 | 0.88085 | 48.172 |

### 5.3.2 Effect on Tensile Stresses in the Casing

As it can be seen in Figure 5.7 below, the shape of the curve of Depth vs Tensile stress for a wellbore of 100m length, is similar to that of 300m length (see Figure 5.3) as well as the maximum tensile stress induced in the casing ($\sim$ 400 MPa). Interestingly, it can be seen that the depth of the casing behaving plastically for each case of $R_i$ has the same magnitude as that for wellbore of $L = 300$m for the same $R_i$. Table 5 summarizes the plastic region of the casing for each case of $R_i$ for both lengths of the wellbore.

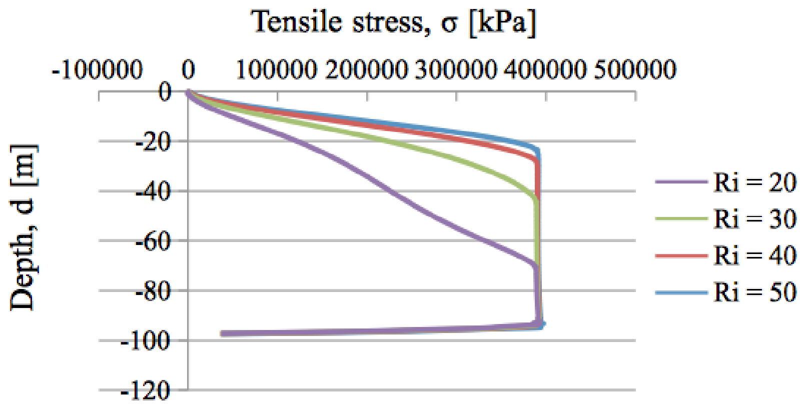


Figure 5.7: Tensile stresses induced in an elastoplastic casing for $L = 100m$

Table 5: Formation profile characteristics for different $R_i$

| $R_i$ [m] | $L$ [m] | $d_{pl}$ [m] |
|---|---|---|
| 20 | 100 | 29.9 |
| 20 | 300 | 27.8 |
| 30 | 100 | 57.5 |
| 30 | 300 | 54.6 |
| 40 | 100 | 72.5 |
| 40 | 300 | 75 |
| 50 | 100 | 77.0 |
| 50 | 300 | 102 |

However, it can be seen that for $R_i = 50$m the depth of the plastic region is not the same for both lengths. For $L = 300$m the plastic region of the casing is 100m whereas for $L = 100$m this is $\sim$ 80m. It can be seen from Figure 5.7 that for increasing $R_i$ the increase of the plastic region becomes less and less. This means that at $\sim R_i = 50$m the increase of the plastic region will not be significant even if $R_i$ increases considerably due to probably boundary effects.

From both sections 5.3.1 and 5.3.2, it can be concluded that the length of the wellbore has no significant effect on the formation settlement profiles or on the length of the casing behaving plastically.

## 5.4 Soil Compression Characteristics

The effect of three different values of $\lambda$ (= 0.8, 0.55, 0.2) on the formation settlement profile and the tensile stresses induced in the casing was examined for constant $\kappa = 0.05$. The same was done for three different values of $\kappa$ (= 0.05, 0.01, 0.004) for constant $\lambda = 0.15$. The results and observations obtained are given in the following sections.

### 5.4.1 Effect on Settlement Profile

Figure 5.8 (a) shows that for a decreasing value of $\lambda$, the maximum settlements, $S_{max}$ are also decreased. This is also observed for a decreasing value of $\kappa$ (Figure 5.8 (b)). However, it is not clear from the graphs whether the trough width, $i$, also decreases and hence the formation settlement profile characteristics are summarised in Table 6 for convenience.

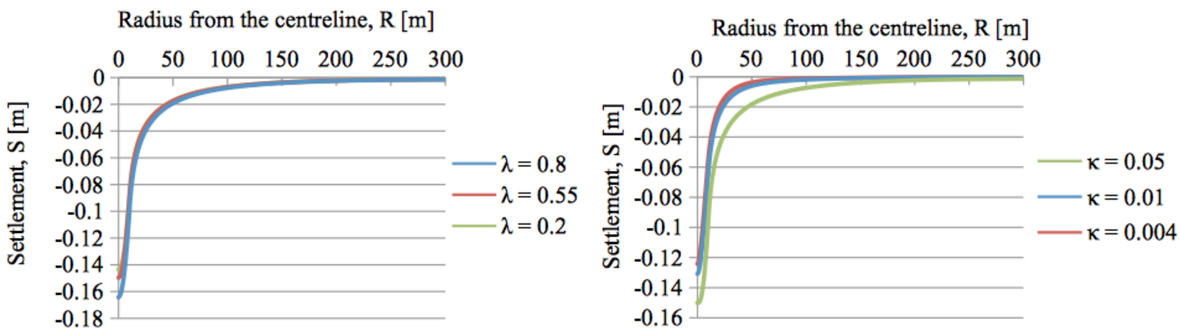


(a) Settlement profile for $\kappa = 0.05$ (b) Settlement profile for $\lambda = 0.15$

Figure 5.8: Effect of $\kappa$ and $\lambda$ on the formation settlement profiles for an elastoplastic casing with $R_i = 10$m and $L = 300$m

For the case of constant $\kappa$, it can be seen that the trough width also decreases with decreasing $\lambda$ and the same is observed for the cases of decreasing $\kappa$. Therefore, increasing $\lambda$ or $\kappa$ would produce more severe results on the behaviour of the wellbore since both $S_{max}$ and $i$ increase in the same sense.

Table 6: Formation Settlement Characteristics for varying $\lambda$ and $\kappa$

| Parameter | $S_{max}$ [m] | $i$ [m] |
|---|---|---|
| **Constant value of** $\kappa = 0.05$ | | |
| $\lambda = 0.8$ | -0.164575 | 10.1303 |
| $\lambda = 0.55$ | -0.149985 | 9.66896 |
| $\lambda = 0.2$ | -0.1431 | 9.2041 |
| **Constant value of** $\lambda = 0.15$ | | |
| $\kappa = 0.05$ | -0.15022 | 9.66437 |
| $\kappa = 0.01$ | -0.143496 | 9.214 |
| $\kappa = 0.004$ | -0.137363 | 7.98989 |

### 5.4.2 Effect on Tensile Stresses in the Casing

As shown in Figure 5.8 above, increasing values of $\lambda$ and $\kappa$, correspond to increasing settlements. Consequently, this would mean that greater stresses along the casing are developed. Figures 5.9 (a) and (b) show that by increasing the value $\lambda$ and $\kappa$, each one independently, the region of the casing that behaves plastically slightly increases. This means that the casing experiences larger stresses, which confirms the expectations.

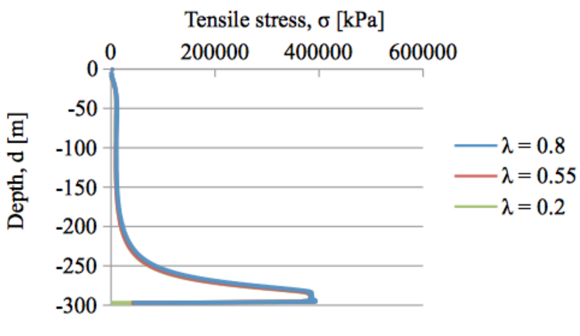


(a) Tensile stress for $\kappa = 0.05$

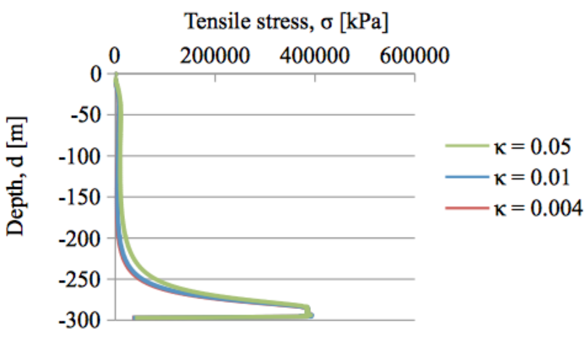


(b) Tensile stress for $\lambda = 0.15$

Figure 5.9: Effect of $\kappa$ and $\lambda$ on the tensile stresses induced in the casing for an elasto-plastic casing with $R_i = 10$m

## 5.5 Settlement profile - Casing Interrelationship

Following the above investigations and results, it was decided to create a plot that would be useful to find out the depth of the casing behaving plastically, for different formation settlement profile characteristics. The graph variables would be the maximum settlement $S_{max}$, the trough width $i$ and the depth of the casing that enters the plastic region $d_{pl}$. Since there are three variables, a contour plot had to be made and it was decided that the contours of constant values would represent the depth of the plastic region of the casing. Furthermore, to generalise the contour plot, all three variables were non-dimensionalised by dividing the variable with the diameter (where D = 0.224m in the model) of the well, since all variables have units of distance.

As already discussed in previous chapters, the critical cases that would induce differential settlements in the casing, are those with large settlements and small values of $i$. However, problems were encountered during implementation of the graph, mostly because the data obtained were only capturing a small range of possible outcomes. For small values of $R_i$, the graph was initially showing only cases of small settlements.

Figure 5.10 shows the initial data points obtained and the trends observed. The graph shows three main features:

1. an inclined line
2. a turning point
3. an almost vertical line

It is assumed that each of the input parameters somehow affects these features, therefore further investigations were then needed to find the effect of each input parameter on the trends observed in order to be able to complete the graph with the data capturing a larger range of outcomes.

Input parameters that would affect the results were assumed to be (a) the amount of pore pressure reduction, $\Delta$u, (b) the distance of pore pressure reduction, $R_i$ and (c) the stiffness of the soil which can be represented by the dimensional numbers $\kappa$ (swelling parameter) and $\lambda$ (compression parameter). Each one of these parameters is investigated independently.

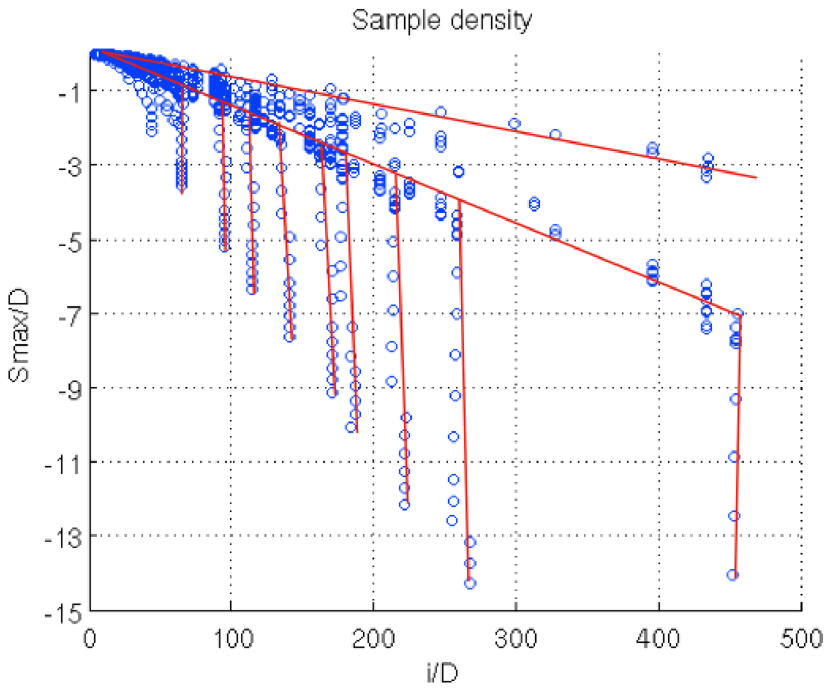


Figure 5.10: The trends observed with the initial data points obtained

### 5.5.1 Effect of Pore Pressure Reduction (Δu)

The data points obtained initially were with a pore pressure reduction of 10 000 kPa in steps of 1000 kPa. This was then changed to a reduction of 26 000 kPa by either increasing the number of steps or by increasing the step reduction depending on which was most computationally effective for each case of different $R_i$. Figure 5.11, shows a plot of the data points obtained for both the cases of $\Delta u = 10000$ kPa and 26000 kPa.

It can be seen from Figure 5.11 that as the pore pressure reduction increases, the amount of settlement also increases as expected. This is because the amount of de-pressurization affects the amount of compaction of the formation and consequently the amount of settlement of the wellbore. Moreover, it can be seen that the curve changes its inclination with increasing pore pressure reduction. By increasing the Δu, the third feature of Figure 5.10 appears. This is further investigated by comparing the effect of different values of $R_i$.

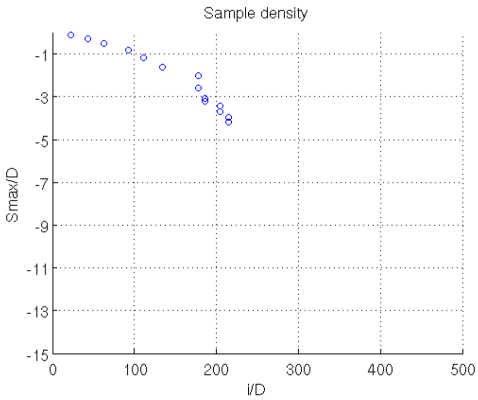


(a) Pore pressure reduction of 10 000 kPa

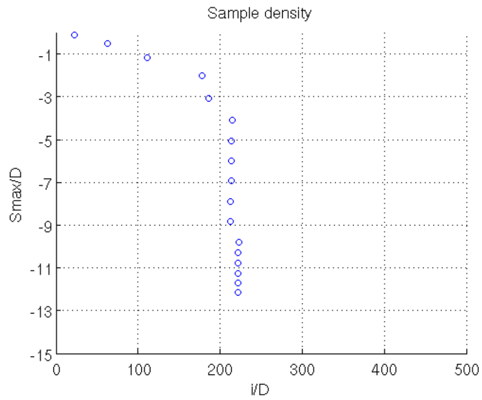


(b) Pore pressure reduction of 26 000 kPa

Figure 5.11: The effect of pore pressure reduction for $R_i = 50$m

### 5.5.2 Effect of Distance of Pore Pressure Reduction ($R_i$)

The data points obtained for the case of pore pressure reduction of 26 000 kPa and $R_i = 50, 100$m are plotted and shown in Figure 5.12 below. It can be seen that the the value of $R_i$ used, affects the position of the turning point on the curve. The result is reasonable as through the input file, the distance of pore pressure reduction is restricted by $R_i$, therefore giving an increasing $S_{max}$ for a constant value of $i$. This observation is very helpful for the implementation of the contour plot as by varying $R_i$ the data points obtained will cover a large range of the x-axis ($i/D$) of the graph.

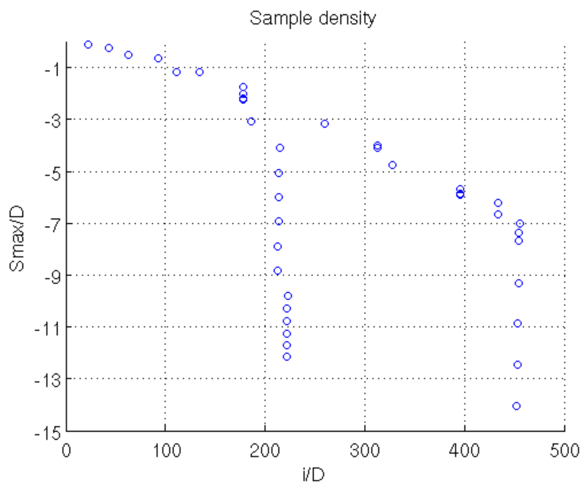


Figure 5.12: The effect of $R_i$, the distance of pore pressure reduction

### 5.5.3 Effect of Swelling Parameter ($\kappa$) and Compression Parameter ($\lambda$)

Three values of $\kappa$ were used initially, $\kappa = 0.01, 0.03, 0.05$ and analyses were made with different values of $R_i$ each time. The data points obtained, were found to lie on distinct lines of different inclination (feature 1.). As it can be seen in Figure 5.13, a smaller value of $\kappa$ produced a line of a shallower gradient. Going back to section 2.2 and Figure 3.3 it can be seen that a smaller value of $\kappa$ corresponds to a larger stiffness of the formation. Therefore during depressurization smaller settlements are expected as shown in Figure 5.13, which confirms the theoretical expectations.

The examination of the effect of $\lambda$ on the contour plot, led to the conclusion that it only affects the maximum settlement obtained and only very slightly the value of $i$, the trough width. Therefore, the differences on the contour plot were found to be negligible.

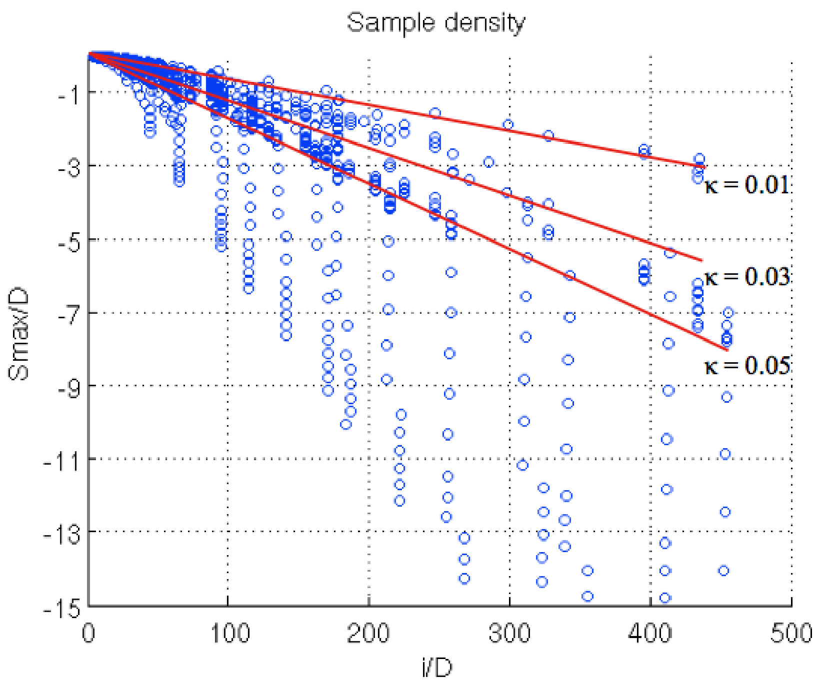


Figure 5.13: The effect of $\kappa$, the swelling parameter

### 5.5.4 Contour Plot

To create a complete contour plot many analyses had to be made and a lot of data had to be collected. Some data were found not capturing different areas of the contour plot or not capturing a greater deformation of the wellbore, so were excluded. The

Table 7: Summary of the input parameters used for the analyses

| No. | $\kappa$ | $\lambda$ | $\Delta$u [kPa] | $R_i$ [m] |
|---|---|---|---|---|
| 1 | 0.05 | 0.2 | 10 000 | 10, 15, 20, 25, 30, 35, 40, 50, 60, 100 |
| 2 | 0.05 | 0.55 | 10 000 | 10, 15, 20, 25, 30, 35, 40, 50, 60, 100 |
| 3 | 0.05 | 0.8 | 10 000 | 10, 15, 20, 25, 30, 35, 40, 50, 60, 100 |
| 4 | 0.01 | 0.15 | 10 000 | 10, 15, 20, 25, 30, 35, 40, 50, 60, 100 |
| 5 | 0.004 | 0.15 | 10 000 | 10 |
| 6 | 0.05 | 0.8 | 18 000 | 10, 15, 20, 25, 30, 35, 40, 50, 60, 100 |
| 7 | 0.03 | 0.8 | 18 000 | 70, 80, 85, 90 |
| 8 | 0.05 | 0.95 | 26 000 | 5, 10 |
| 9 | 0.05 | 0.8 | 26 000 | 10 |
| 10 | 0.09 | 0.95 | 26 000 | 5, 10 |
| 11 | 0.07 | 0.95 | 26 000 | 15, 20 |
| 12 | 0.06 | 0.95 | 26 000 | 25, 30 |

parameters used for each of the analyses made (for the data that were included at the end) are summarised in Table 7.

Figure 5.14 shows a graph of $S_{max}/D : i/D : d_{pl}/D$, where the contours show the boundaries of each region of constant $d_{pl}/D$. There is a clear trend of increasing values of $S_{max}/D$ for decreasing values of $i/D$ and for constant $d_{pl}/D$ and this increase becomes more abrupt for small values of $i/D$. This shows that for a given value of $i$, as $S_{max}$ increases so does the depth of the plastic region, which is as expected. However, for a given $S_{max}$, as $i$ increases, $d_{pl}$ also increases. This result is not straightforward at the first instance, because for increasing $i$ and therefore wider settlement profile, we would expect a uniform settlement of the wellbore and hence reduced plastic region. However, by increasing $i$ it is recognised that the volume of the soil that settles increases and therefore corresponds to increase plastic region in the casing.

This created the need to produce a different graph which could be used to assess the stress state of the elasto-plastic casing when the characteristics of the formation settlement profile at the final stage of the depressurization are known. Instead of plotting $S_{max}/D$ on the y-axis, $log$(Volume of formation settlement profile/Volume of a semi-sphere of diameter D) is used.

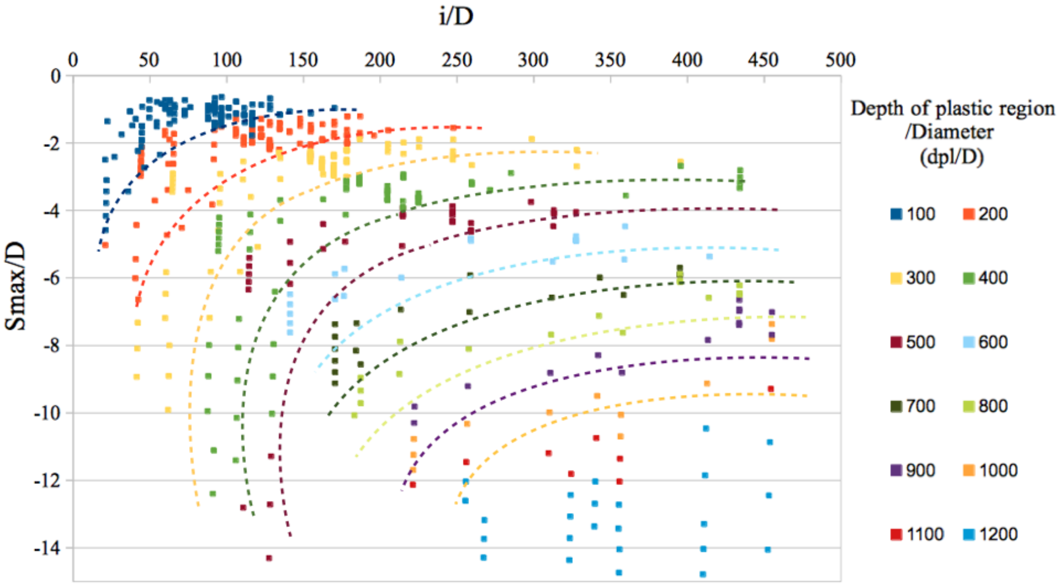


Figure 5.14: Contour plot of $S_{max}/D : i/D : d_{pl}/D$ for $L = 300$m

It was observed that the settlement profile follows a Gaussian function. Thus, the volume under the Gaussian function assuming axisymmetric conditions was used to compute the settlement volume of the formation settlement profile, as follows:

$$V = \int_{-\infty}^{\infty} \int_{-\infty}^{\infty} f(x,y)dxdy = 2\pi * S_{max} * i^2 \tag{5.2}$$

Therefore, instead of considering only the maximum settlement, the total settlement volume during depressurization is considered. This was non-dimensionalised with the volume of a semi-sphere $(\frac{4\pi(D/2)^3}{3} * \frac{1}{2})$ which is the zone below the bottom of the wellbore.

The new contour plot is shown in Figure 5.15. It can be seen that for constant settlement volume and increasing trough width the plastic region of the casing decreases as previously explained. Furthermore, for constant trough width and increasing settlement volume, the plastic region of the casing increases again as expected. Therefore, this graph provides a clearer representation of the behaviour of the formation during depressurization.

In order to confirm that this graph would serve as a guidance for the design of a wellbore, the contour plot was checked with data obtained for a wellbore of 100m length. As it can be seen in Figure 5.16, points lie within the correct boundaries.

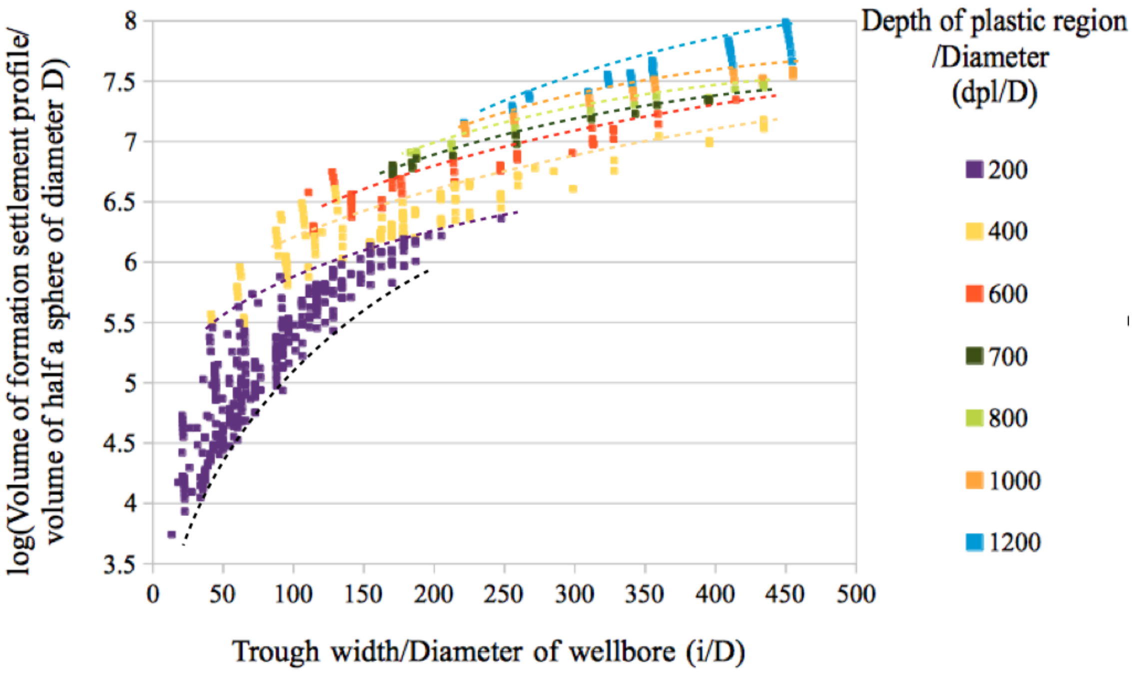


Figure 5.15: Contours of constant $d_{pl}/D$ for $L = 300$m

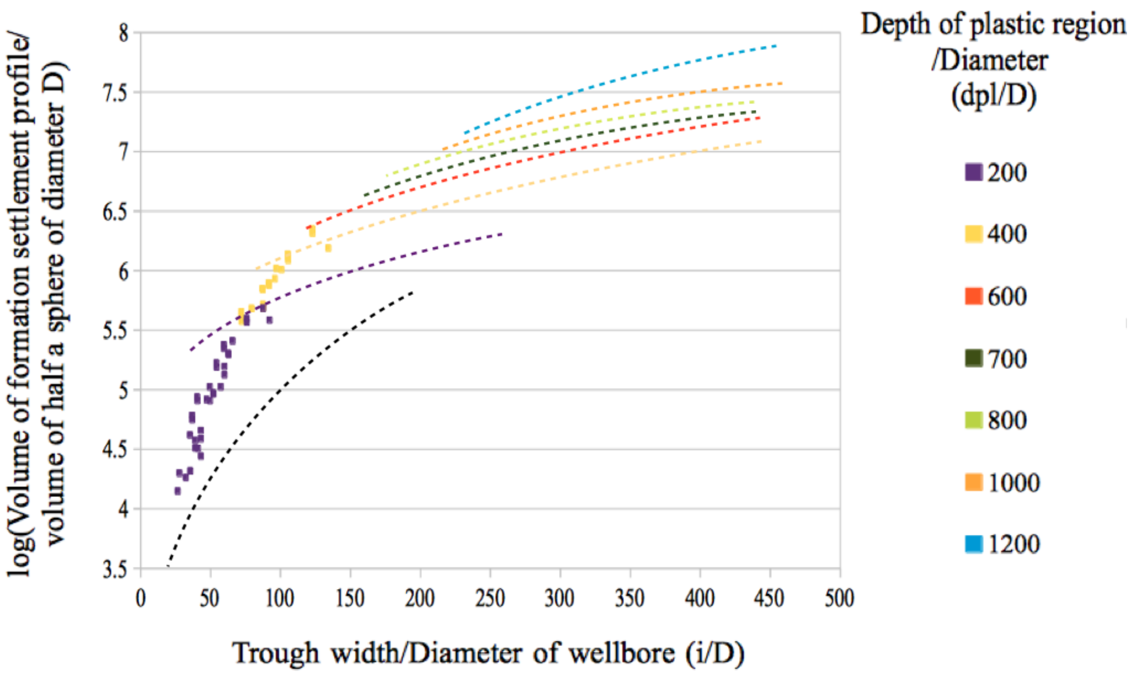


Figure 5.16: Contours of constant $d_{pl}/D$ for $L = 100$m

# 6 Conclusions and Recommendations for Future Research

Due to the large amount of methane gas found in hydrate-bearing sediments worldwide and the fact that it is a highly energy intensive fuel, methane gas has been recognised as a potential energy resource.

However, in order to extract the gas, the hydrate needs to be dissociated through changes of pressure and temperature conditions, therefore, many geomechanical challenges are raised. These include well instability and casing deformation which must be investigated in great depth before any gas production can be extensively developed

Although it has been recognised that methane hydrates have an important role in the ongoing global carbon cycle and climate change, deposits that are currently targeted for gas production, are found in sand reservoirs that exist deeply buried in the subsurface and are thought to be environmentally non-critical. As discussed by Moridis et al., (2009), these deposits are closer to the stability conditions for gas hydrates.

From the finite element model and study made by E. Xu (2014) it was established that the proposed constitutive and computational models can adequately simulate case-study results. It was then found that during depressurization the hydrate sediments undergo considerable compaction especially in the near-wellbore region affecting the wellbore structural integrity and stability.

In this study, the possible parameters affecting wellbore's stability and integrity were investigated in order to identify those with considerable effect on the formation compaction profiles of the hydrate sediments and on the tensile stresses in the casing. It was found that the length of the wellbore and the elasto-plasticity of the casing did not have any significant effect on the formation settlement profiles. Tensile stresses in the casing were not affected by wellbore lengths, but were reduced when the elasto-plasticity of the casing was considered.

On the other hand, the distance of pore pressure reduction and the soil compression characteristics were found to affect the formation settlement profiles, as well as the tensile stresses in the casing. The tensile stresses were found to increase with increasing distance of pore pressure reduction. Larger distance of pore pressure reduction although created larger settlements, it also gave wider formation settlement profiles. These settlement profiles were found to be less critical for the wellbore integrity and stability because they cover a large region away from it and hence the wellbore displaces uniformly, compared with those of smaller distance of pore pressure reduction which induce differential settlements in the wellbore. When the increase of pore pressure reduction was examined in conjunction with an elasto-plastic casing material the depth of the casing behaving plastically also increased.

The soil compression characteristics, $\kappa$ and $\lambda$, when increased one by one, were found to slightly increase the maximum settlement of the wellbore as well as the trough width of the settlement profile and the plastic region of the casing.

The final objective was to examine the interrelationship of the tensile stresses in the casing and the formation settlement profile characteristics. Since the maximum tensile stress in the casing was found to remain the same for any changes of other parameters, the relationship of the depth of the plastic region of the casing, the settlement volume and the trough width of a settlement profile was decided to be found. Dimensionless numbers were used to generalise the problem and a contour plot was created. Curves of the same trend were generated which show that for constant settlement volume and increasing trough width, plastic region decreases whereas for constant trough width and increasing settlement volume, plastic region increases. It is therefore concluded, that not only maximum settlement but also the settlement volume is an important parameter for the stress condition of the casing.

It is hoped that these curves will be further validated through additional complimentary research so that they can possibly be used for wellbore assessment. Possible future work could also include the investigation of parameters that would cause additional stresses in the casing due to radial differences in soil or pressure conditions (non-axisymmetric conditions). In this study the depressurization process is interpolated at each time step, however the behaviour of the wellbore could influence the pore pressure change. Therefore, a simulation which could capture the coupled behaviour should be considered in the future. Moreover, the investigation of an inclined or horizontal wellbore could also be considered.

# Acknowledgements

I would like to thank Professor Kenichi Soga, for his direction, challenging discussions, constructive criticism and continuous involvement in every aspect of this research.

I would like to express my appreciation to Tsubasa Sasaki for his invaluable guidance, cooperation and assistance in the use of the software ABAQUS.

I would like to thank Ermao Xu and Mingliang Zhou for cooperating and assisting in the use of the Finite Element Model on ABAQUS.

Finally, I am deeply indebted to my family for their continuous love and support.

# References

[1] K.A. Kvenvolden. “A primer in gas hydrates, in Howell, D.G., ed., The Future of Energy Gases”. In: *U.S. Geological Survey Professional Paper 1570* (1993), pp. 279–292.

[2] T.S. Collett. “Energy resource potential of natural gas hydrates”. In: *AAPG Bull. 86 (11): 1971-1992* (2002).

[3] R. Boswell and T.S. Collett. “Current status of gas hydrate resources”. In: *Energy and Envrionmental Science* (2010). DOI: 10.1039/c0ee00203h.

[4] H.H. Sisler, R.D. Dresdner, and W.T. Mooney. “Chemistry a Systematic Approach”. In: *Oxford University Press* (1980).

[5] H. P. Greenspan. “Supplementary Paper on Methane Hydrates”. In: *MITEI Natural Gas Report* (2011).

[6] K. Soga et al. “Numerical Analysis of Wellbore Behaviour during Methane Gas Recovery from Hydrate Bearing Sediments”. In: *Offshore Technology Conference* (2014).

[7] E. Xu. “Numerical Analysis of Wellbore Behaviour during Methane Gas Recovery from Hydrate Bearing Sediments”. PhD thesis. University of Cambridge, 2014.

[8] S. Uchida, K. Soga, and K. Yamamoto. “Critical state soil constitutive model for methane hydrate soil”. In: *Journal of Geophysical Research* VOL. 117, B03209 (2012). DOI: 10.1029/2011JB008661.

[9] K.A. Kvenvolden. “Methane hydrate–A major reservoir of carbon in the shallow geosphere?” In: *Chem. Geo. 71* (1988).

[10] S.K. Garg et al. “A mathematical model for the formation and dissociation of methane hydrates in the marine environmen”. In: *J. Geophys. Res., 113, B01201* (2008). DOI: 10.1029/2006JB004768.

[11] R.J. Davies et al. “Oil and gas wells and their integrity: Implications for shale and unconventional resource exploitation”. In: *Marine and Petroleum Geology 56, 239-254* (2014).

[12] G.J. Moridis et al. “Challenges, Uncertainties and Issues Facing Gas Production From Gas Hydrate Deposits”. In: *SPE Reservoir Evaluation and Engineering, SPE-13179* (2010).

[13] J. Rutqvist, T. Grover, and G.J. Moridis. “Coupled Hydrological, Thermal and Geomechanical Analysis of Wellbore Stability in Hydrate-Bearing Sediments”. In: *OTC 19672, Proc. 2008 Offshore Technology Conference, Houston, 4-8 May* (2008).

[14] J. Rutqvist and G.J. Moridis. “Numerical Studies on the Geomechanical Stability of Hydrate-Bearing Sediments”. In: *SPE 126129. SPE J. 14:* (2009), pp. 267–282.

[15] G. Dickens. “Rethinking the global carbon cycle with a large, dynamic, and microbially mediated gas hydrate capacitor”. In: *Earth and Planetary Science Letters 213* (2003), pp. 169–183.

[16] G. Dickens et al. “Dissociation of oceanic methane hydrate as a cause of carbon isotope excursion at the end of the Paleocene”. In: *Paleooceanography 10* (1995), pp. 965–971.

[17] IPCC. *Climate Change 2007: The Physical Science Basis: Intergovernmental Panel on Climate Change.* Tech. rep. IPCC, 2007.

[18] G.J. Moridis and M.T. Reagan. “Gas Production From Oceanic Class 2 Hydrate Accumulations”. In: 2007.

[19] G.J. Moridis et al. “Toward production from gas hydrates: assessment of resources and technology and the role of numerical simulation”. In: *SPE 114163, SPE J., 12 (5)* (2009), pp. 745–771.

[20] M. Salehabadi et. al. “Finite Element Modelling of Casing in Gas Hydrate Bearing Sediments”. In: *In SPE Europec/EAGE Annual Conference and Exhibition. Rome, Italy* (2008).

[21] J. Rutqvist et al. “Coupled Multiphase Fluid Flow and Wellbore Stability Analysis Associated with Gas Production from Oceanic Hydrate-Bearing Sediments”. In: *Journal of Petroleum Sciences and Eng.92-93* (2012), pp. 65–81.

[22] A. Klar, K. Soga, and M.Y. Ng. “Coupled DeformationFlow Analysis for Methane Hydrate Extraction”. In: *Geotechnique, 60(10)* (2010), 765776.

[23] s. Kimoto, F. Oka, and T. Fushita. “A chemothermomechanically coupled analysis of ground deformation induced by gas hydrate dissociation”. In: *SPE Journal* (2010), pp. 21–23.

[24] J. Kim et al. “Numerical Studies on Two-Way Coupled Fluid Flow and Geomechanics in Hydrate Deposits”. In: *International Journal of Mechanical Sciences, 52(2)* (2012), 365376.

[25] K. Soga et al. “Characterization and engineering properties of methane hydrate soils”. In: 2nd International Workshop on Characterization and Engineering Properties of Natural Soils. Natl. Univ. of Singapore, Singapore, 2006.

[26] *Fire in The Ice.* Issue 2 Methane Hydrate Newsletter, Vol.13, National Energy Technology laboratory, U.S Department of Energy. 2013.

[27] R. Boswell. “Fire in the Ics”. In: *Methane Hydrate Newsletter, 13(2)* (2013).

[28] S. Uchida et al. “Geomechanical study of the Mallik gas hydrate production field trials”. In: *Geological Survey of Canada Bulletin 601, pp1-2.* (2012).

[29] *Abaqus Documentation.* 6.13. Simulia.

[30] K.H. Roscoe, A.N. Schofield, and C.P. Wroth. “On the yielding of soils”. In: *Geotechnique* 8(1) (1958), pp. 22–53.

# A Risk Assessment Retrospective

The project complies with all health and safety standard procedures with proactive measurements taken from the beginning to the end.

The project did not involve any experimental work, instead it was completely computational. Therefore, the major concern that could affect the health of the student was the excessive use of the computer.

However, protective measures were overtaken in order to avoid any of the computer-overuse consequences. The student was using a proper workstation design and was trying to keep a good posture throughout the hours spend in front of the computer. The computer screen was adjusted to be slightly lower than eye level and the chair was adjusted so that the feet were rest flat on the floor.